The Effects of Anthropogenic Land Use Changes on Climate in China Driven by Global Socioeconomic and Emission Scenarios

Na Dong[1] (iD), Zhen Liu[2,3], Ming Luo[3,4] (iD), Chaoyang Fang[5], and Hui Lin[1,5,6] (iD)

[1]Institute of Space and Earth Information Science, The Chinese University of Hong Kong, Shatin, Hong Kong, [2]School of Geosciences, The University of Edinburgh, Edinburgh, UK, [3]Institute of Environment, Energy and Sustainability, The Chinese University of Hong Kong, Shatin, Hong Kong, [4]School of Geography and Planning, and Guangdong Key Laboratory for Urbanization and Geo-simulation, Sun Yat-sen University, Guangzhou, China, [5]School of Geography and Environment, Jiangxi Normal University, Nanchang, China, [6]Shenzhen Research Institute, The Chinese University of Hong Kong, Shenzhen, China

Abstract The land surface, which interacts with lower atmosphere, is subject to substantial amounts of human activities. It results in regional climate fluctuations and must be assessed with a combination of future socioeconomic and emission policies to improve regional resilience and responsive efficiency on global mitigation and adaptation. Spatial heterogeneity in regional climate induced by land use changes of future global socioeconomic and emission scenarios is explored. Comparisons are carried out among both historical and future land use-induced regional meteorological changes to investigate various climatic roles of land use conversions in China. The underlying changes in the surface albedo, leaf area index, energy exchange, and water balances are also examined. It is found that the increase of the summer temperature and the diurnal temperature range are the largest under the fifth Shared Socioeconomic Pathway characterized by more intensive urbanization. While temperature increase from urbanization and deforestation can be offset by cooling from vegetation evaporation increase under the extreme Representative Concentration Pathway (RCP) 8.5, which has no climate mitigation policies and high greenhouse gas concentration. In addition, RCP4.5 scenario would cause an average temperature increase of 1.41°C by 2050 at an annual rate of 0.028°C in China. The global climatic forcing warms the entire region and enhances precipitation intensity, and these effects are more substantial than those by regional land use changes, showing a strong background influence. Our research reveals the future climatic responses to regional anthropogenic land use changes under various scenarios and policies and provides ways to downscale global mitigation impacts into regional insights.

1. Introduction

A regional analysis reported that anthropogenic land use has increased by approximately 48.5%, transforming natural biomes due to diverse anthropogenic activities since 1750 (Lawrence & Chase, 2010). Because of global demands for energy, water, and food, land use and land cover, for example, croplands, urban, and pasture areas have expanded at the cost of biodiversity losses and natural vegetation degradation (Foley, 2005). Although the land surface-induced global climate changes are not significantly captured, anthropogenic land surface processes such as urbanization, the conversion of midlatitude natural forests to cropland and pastures, wood harvesting, and shifting cultivation in the tropics have been validated as exerting remarkable effects on regional climate extremes through surface energy partitioning and water balance (Pielke et al., 2007; Mahmood et al., 2010; Findell et al., 2017). Furthermore, socioeconomic changes such as population growth, rapid economic development, and industrialization modes are accelerating the urbanization process and gradually becoming critical factors that trigger environmental changes, especially for land use resources.

Land use change has contributed to 15% of total carbon emissions from 1990 to 2010 in China, and anthropogenic land use conversions have altered physical characteristics of the land surface (Lai et al., 2016). It has been noted that large-scale land use changes would affect the mean regional climate and increase the risk of climate extremes (De Noblet-Ducoudré et al., 2012; Fall et al., 2010; Mahmood et al., 2008; Teuling et al., 2010). For natural biome changes, China has experienced the greatest decrease in temperate and mixed forests, accounting for 36.6% of the land and another 14.9% losses of gross tropical forests, savanna, grasslands,

and shrublands due to human disturbance (Lawrence & Chase, 2010). However, the latest finding shows that the Earth suffers prominently greening of which China account for a total 25% net increase in green leaf area from 2000 to 2017 mainly attributable to cropland greening (Chen et al., 2019). The increasing impervious surface and decreasing vegetation cover changed regional and local climate by affecting energy, momentum, and matter exchange between land surfaces and the atmosphere (Argüeso et al., 2014; Cao et al., 2016; Feng et al., 2012; Oleson et al., 2015; Ren et al., 2008), leading to typical regional climate anomalies such as the Urban Heat Island and reductions in the local diurnal temperature ranges (DTR; Zhou et al., 2004; Hale et al., 2006, 2008; Luo & Lau, 2017).

The biogeophysical effects of land use changes on climate have higher uncertainty than biogeochemical effects (De Noblet-Ducoudré et al., 2012) and contribute less to the changes of the global radiative forcing than other climate forcings (Rounsevell et al., 2014). Nevertheless, human activities now appropriate nearly one third to one half of global ecosystem production (Foley, 2005), which were partly converted from midlatitude forests. It would either lead to cooler winter (Govindasamy et al., 2001; Matthews et al., 2003; Roy et al., 2007) or warmer summer (Jeong et al., 2014) by increasing albedo in Northern China. Reforestation and afforestation affect biogeophysical and biogeochemical features of land cover and therefore bring great uncertainties to regional climate. A warmer, drier climate is occurred when facing extensive clearing of tropical forests (Bonan, 2008; Costa & Foley, 2000), whereas cooling effects are expected by increased albedo in the case of the large decrease in temperate and boreal forests (Bonan et al., 1992; Brovkin et al., 2006; Davin & de Noblet-Ducoudre, 2010). Therefore, land use change effects should be seriously evaluated by integrating with regional climate model such as the Weather Research and Forecasting (WRF) model (Skamarock et al., 2008) to deepen the understanding of changes in albedo, energy partitioning, and turbulent flux exchanges for water and heat, as well as to further improve human capabilities to efficiently mitigate anthropogenic land use impacts.

With the proposal of the International Panel on Climate Change's Fifth Assessment Report (International Panel on Climate Change Fifth Assessment Report, 2013), various socioeconomic and emission pathways, the Shared Socioeconomic Pathways (SSPs) and Representative Concentration Pathways (RCPs; Moss et al., 2010; O'Neill et al., 2014, 2017; van Vuuren et al., 2011), involved with new technologies and policies are promoted to strengthen the capabilities of humans to cope with future challenges and adaptations (Hurtt et al., 2011; van Vuuren et al., 2011). Improving the understanding of the relationship between land use and climate dynamics based on global socioeconomic and climatic assumptions plays a crucial role in regional climate monitoring and achieving the global mitigation target. Therefore, tremendous pressures on more reasonable and effective assessment methods to simulate potential effects of anthropogenic land use change on climate are to rise. The combination of global scenarios with regional environmental dynamics provides quantitative interpretations to the top-down global assessments and bottom-up human-environmental interactions across multiple scales (Pielke & Niyogi, 2010). The evaluation of potential anthropogenic land use changes and their regional environmental impacts driven by global sustainable strategies in the long term increases the resilience of managed landscapes and broadens the foresight for city planners and decision makers.

Previous research has examined the impacts of land use changes on regional climate over historical periods (Cao et al., 2016; Lin et al., 2016) as well as the future. These studies are always based on idealized assumptions of possible conversions or fixed indications of land-type changes. The global RCP scenarios have been applied as the driving forces to evaluate the future impacts of global and regional climatic changes caused by specific land use conversions (Table 1). However, these scenarios concerned the impacts of a single land use type such as urbanization (Adams et al., 2015; Chen & Frauenfeld, 2016; Yang et al., 2016) or the relationship between land use and climatic factors without considering the internal driving elements of anthropogenic policies and societal factors. Deng's group (Deng et al., 2014; Li et al., 2013) have evaluated the future temperature changes that are expected to result from grassland degradation in Inner Mongolia and increased cultivated lands in Northeast China under the RCP6.0 scenario from 2010 to 2050. Ward et al. (2014) also calculated land use-derived emissions and radiative forcing under various RCP scenarios. However, associated socioeconomic activities and climatic policies from the global scenarios are not included and explained in those frameworks.

Hence, to enable the predictive understanding of future climate change, the interactions between land use and climate should be assessed in the context of anthropogenic activities, which can be promoted by the

Table 1
Global Scenarios Based on Land Use Change and Climate Simulation in China

Research	Scenario	Region and spatial resolution	Land-use type	Simulation period	Climate model	Meteorological factors
Deng et al. (2014) and his group	RCP6.0	Northwestern China, Inner Mongolia, 30 km	Grassland, cultivated land	2040-2050, 2020	WRF-ARW	T2, P, energy flux
Ward et al. (2014)	RCP2.6, RCP4.5, RCP6.0, RCP8.5	Global	Forest, cropland, pasture	2010-2100	CESM-CLM-CN v3.5, CESM-CAM5	Land use emission
Davies-Barnard et al. (2015)	RCP2.6, RCP 4.5, RCP 8.5	Global	Forest	2005-2100	HadGEM2-ES	Carbon emission
Adams et al. (2015)	RCP4.5	Sydney, 50 km, 10 km, 1 km	Urban	2020-2039, 2060-2079	GCMs driven WRF, TAPM-UCM	T2
Chen and Frauenfeld (2016)	RCP4.5	China, 30 km	Urban	2050-2060	WRF/UCM	T2, P, humidity
Yang et al. (2016)	RCP8.5	Beijing metropolitan	Urban	2050s	WRF/UCM	T2

Note. T2 represents near-surface 2-m temperature, and P represents precipitation. Abbreviations: CESM-CAM5, Community Earth System Model-Community Atmosphere Model version 5; CESM-CLM-CN, Community Earth System Model-Community Land Model-Carbon Nitrogen; GCM, global climate model; HadGEM2-ES, Hadley Centre Global Environmental Model version 2 Earth System; RCP, Representative Concentration Pathway; TAPM-UCM, The Air Pollution Model Urban Canopy Model; WRF-ARW, Weather Research and Forecasting-Advanced Research WRF.

conjoint analysis of global socioeconomic and emissions scenarios. In this study, we construct a framework combining land use data, concerning the socioeconomic and emission factors from the global SSPs and RCPs, and regional climate model to evaluate the possible effects of land use on the regional climate. The comparisons are made among the climatic patterns induced by both historical and future land use changes as well as among the climatic roles of various land use conversions among different scenarios. Meanwhile, the interactions between land use changes and regional climate changes are further revealed with respect to different forcings (the only land use induced and the non–land use induced). The sensitivity of regional climate to multiple societal development and climatic policies is also examined to enhance the understanding of uncertainty and variability of climate related to future policy and management decisions.

2. Model Description and Experimental Design
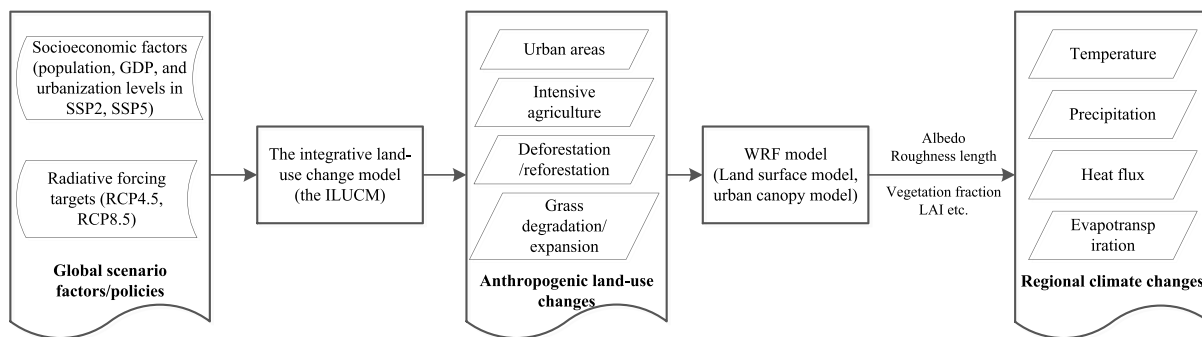
2.1. Conceptual Framework

To explore the multiple global effects of land use changes on regional climate, a scenario-based framework is designed to examine human policy-induced impacts on land use change and climate in China (Figure 1). Two kinds of models are embedded in the entire simulation process. One is the integrative land use change model (ILUCM), which is constructed and applied in Dong et al. (2018), to assess the anthropogenic land use changes and future distributions due to global impacts. The other one is the mesoscale WRF model that is widely used to simulate interactions among radiation, turbulence, energy fluxes, and the land surface in special consideration of the urban canyon geometry.

Scenarios of land use induced climate changes considering both socioeconomic factors (e.g., population, gross domestic product (GDP), and urbanization levels in SSP2 and SSP5) as well as emission policies (e.g., RCP4.5 and RCP8.5) can be built and realized through this framework. In ILUCM, anthropogenic effects of emission and socioeconomic element interventions are reflected by regional land use changes of urban areas, agricultural areas, natural vegetation, and barren lands. Then, evaluation of corresponding regional climatic impacts is assessed through the WRF model at a finer resolution. In this way, future land use-induced regional variation in temperature, precipitation, heat flux, and evaporation, which highly depends on the land surface properties such as albedo, roughness length, and the leaf area index (LAI), can be captured and evaluated.

2.2. The Integrative Land Use Change Assessment Model

The ILUCM, constructed by the Global Change Assessment Model (GCAM; Kim et al., 2006; Clarke et al., 2007) and the future land use simulation model (FLUS; Li et al., 2017; Liu et al., 2017), is adopted in this research to generate spatial future land use data sets under various global socioeconomic and emission scenarios.

Both SSP and RCP pathways are initialized inputs for ILUCM and would be first simulated in GCAM module. Data from SSP scenarios are used to form the future descriptions of demographic, economic, and technological development, while RCP targets are to indicate greenhouse gas (GHG) emission roads by the end of the 21 century. In GCAM, land use demands from 2010 to 2100 would be decided directly by agricultural markets after balancing effects of various policies (e.g., climate policy and energy policy), energy markets, economy levels, and emissions from fossil and industrial and land use on carbon or

Figure 1. The conceptual framework of this research

GHG prices (Wise & Calvin, 2011). Then various trends of land use area pathways considering corresponding impacts of socioeconomic factors of SSPs or climatic policies of RCPs are generated. Utilizing those land use demands based on artificial neural network (ANN) mechanism-based Cellular Automata framework, FLUS module in ILUCM makes it possible to realize land use downscaling from the qualitative amounts to various spatial distributions concerning top-down and bottom-up interactions of global policies and local environment and suitability of conversions among all land use types. All future land use data sets used in this research are produced by ILUCM and some of them have been described in the study of Dong et al. (2018).

2.3. WRF Model and Observational Data

The WRF model is a mesoscale model for numerical weather forecasting and is a data assimilation system (Skamarock et al., 2008). Maintained and supported as a community model to facilitate the wide use for research and teaching in the academic community, it is suitable for applications across scales ranging from meters to thousands of kilometers (Skamarock et al., 2005). The WRF forecasting model (version 3.9.1) is employed to assess the impacts of global scenarios and land use changes driven by global forcings and to improve resolution of physical process and feedback at regional scales (Chen & Frauenfeld, 2016). Land use and land cover are critically relevant to the selected land surface module in WRF, which is the Noah Land Surface Model (LSM; Chen & Dudhia, 2001) with a single-layer Urban Canopy Model (UCM; Kusaka & Kimura, 2004) in this research. Noah LSM has been applied with the WRF model in multiple studies to evaluate the climatic impacts of vegetation, soil moisture, and agricultural crop changes (Chen et al., 2010; Georgescu et al., 2011; Hong et al., 2009). Furthermore, the UCM can capture complex interactions between urban land surfaces and regional atmospheric processes and provide an efficient tool to simulate local urban thermal anomalies (Argüeso et al., 2014; Chen et al., 2011; Grossman-Clarke et al., 2010; Wang et al., 2012).

WRF simulations for both the historical and future periods are performed in a one-way nested domain covering the entirety of China (Figure 2). The domain covers an area with 237 zonal grids and 175 meridional grids using 27-km grid spacing, centering at 36°N and 103°E. The suite of WRF physical parameterizations consists of the WRF Single Moment 3-class microphysics scheme, the Rapid Radiative Transfer Model (RRTM) longwave radiation scheme, the Dudhia shortwave radiation scheme, the MM5 Similarity surface layer scheme, the Unified Noah land-surface Model, the Yonsei University boundary layer scheme, the Kain-Fritsch cumulus physics scheme, and the Noah LSM with the default single-layer UCM.

Meanwhile, two sets of observational data are included to evaluate simulation performance. The Climate Research Unit Time Series (CRU TS) 3.2.1 data set (Harris et al., 2014) at 0.5-degree grid resolution from 1901 to 2015 is used to assess simulation accuracy and correlations. As CRU TS data have long temporal and extensive spatial coverage but relatively coarse resolution, observations from 2,747 in situ observations in China are also adopted to describe more detailed information (see Figure 2).

2.4. Experiment Design and Validation

To quantify the potential impact of different land use changes on regional climate in China, six experiments are designed with four sets of land use data (Table 2). Three control experiments, CTL_2000_LND_2000, CTL_RCP45_2050_LND_2000, and CTL_RCP85_2050_LND_2000, adopt the same historical 2000 land
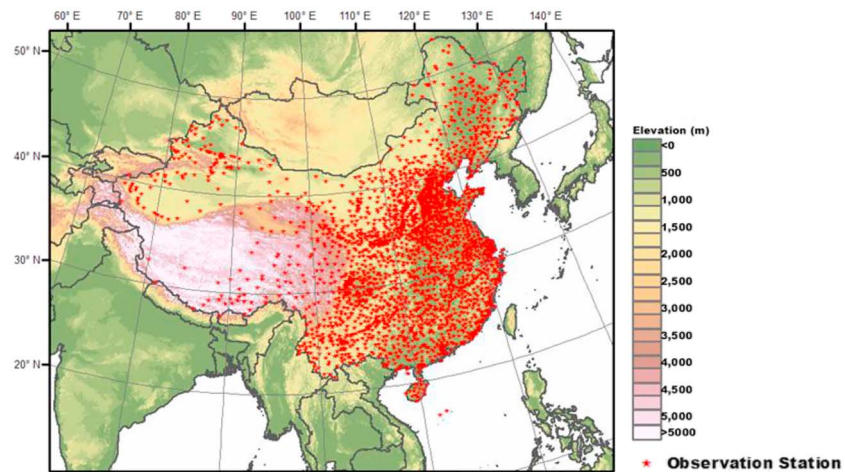
Figure 2. Simulation domain and the 2,474 meteorological observation stations across China used in this research (shown as red stars).

use data but have different initial and boundary (B/I) conditions as CTL_2000_LND_2000 uses the bias-corrected 20th century, while CTL_RCP45_2050_LND_2000 and CTL_RCP85_2050_LND_2000 uses the CMIP5 RCP4.5 forcing and RCP8.5 forcing data (Monaghan et al., 2014), respectively. The climatic condition under RCP4.5 represents a moderate emissions level that stabilizes global radiative forcing at 4.5 W/m^2 in 2100 without exceeding the limit (Thomson et al., 2011). In contrast, RCP8.5 with very high GHG emissions and no specific climate mitigation target leads to a radiative forcing of 8.5 W/m^2 at the end of 21 century (Riahi et al., 2011). Additionally, three future experiments including RCP45_2050_LND_S2_RCP45, RCP45_2050_LND_S5_RCP45, and RCP85_2050_LND_S5_RCP85 employ three 2,050 land use data sets, which are generated by ILUCM with combinations of SSP2, SSP5, and RCP4.5, RCP8.5 pathways, to carry out climate simulations under B/I conditions of RCP4.5 and RCP8.5, respectively. Detailed descriptions of those future scenarios and land use data sets are shown in section 2.5. The simulation periods span three and a half years from July 1998 to December 2001 for CTL_2000_LND_2000 and from July 2048 to December 2051 for the rest five experiments, taking the first half-year as the spin-up period. The averages of those three years in each experiment are used to represent actual climatic variations in the following discussion.

The evaluation of anthropogenic land use change effects are realized from comparisons among three future scenarios (RCP45_2050_LND_S2_RCP45, RCP45_2050_LND_S5_RCP45, and RCP85_2050_LND_S5_RCP85) and control scenarios (CTL_RCP45_2050_LND_2000 and CTL_RCP85_2050_

Table 2
Simulations and Experiments Designed in This Research

No.	Simulation	Land use[a] data sets	Land use descriptions	Initial/boundary conditions
1	CTL_2000_LND_2000	2000	Historical 2000 land use condition	CMIP5 in the 20th century
2	CTL_RCP45_2050_LND_2000	2000		CMIP5 RCP4.5 in the 2050s
3	CTL_RCP85_2050_LND_2000	2000		CMIP5 RCP8.5 in the 2050s
4	RCP45_2050_LND_S2_RCP45	2050 SSP2 and RCP4.5	2050 land use under middle-level economic development and GHG emissions	CMIP5 RCP4.5 in the 2050s
5	RCP45_2050_LND_S5_RCP45	2050 SSP5 and RCP4.5	2050 land-use under rapid economic development and middle-level GHG emissions	CMIP5 RCP4.5 in the 2050s
6	RCP85_2050_LND _S5_RCP85	2050 SSP5 and RCP8.5	2050 land use under rapid economic development and high GHG emissions	CMIP5 RCP8.5 in the 2050s

Abbreviations: CMIP5, Coupled Model Intercomparison Project Phase 5; GHG, greenhouse gas; ILUCM, integrative land use change model; RCP, Representative Concentration Pathway; SSP, Shared Socioeconomic Pathway.
[a]The land use data sets are from the existing data set such as historical 2000 or generated from the ILUCM constrained by the different combinations of SSP and RCP scenario trends as described in detail in Dong et al. (2018). Detail generation methods for three future land use data sets are elaborated in Text S1 in the supporting information.

LND_2000) with historical land use distributions from 2000. Various levels of human intervention on regional climate from land use change can be revealed from either socioeconomic or emission aspect. Other than land use impacts, climatic forcing impact, closely related to background B/I conditions adopted in the experiment, is another dominant factor for regional climate and would be explored through comparisons. Significant t test s are conducted for each climatic variation using the common significance level of 0.05 to show the actual significant changes between those scenarios. In all, three kinds of comparisons are implemented in this research:

1. Future climatic effects from land use changes by comparing control experiments (CTL_RCP45_2050_LND_2000 and CTL_RCP85_2050_LND_2000) and the three future scenarios (RCP45_2050_LND_S2_RCP45, RCP45_2050_LND_S5_RCP45, and RCP85_2050_LND_S5_RCP85) separately, with groups of experiments using climatic forcing at consistent levels in the 2050s, but different land use distributions; detailed comparisons and results are displayed in sections 3.2 and 3.3.
2. Different climatic roles of various land use conversions among scenarios by comparing the separate land use change fractions to the total land use changed areas and their corresponding temperature changes induced by those various land use types; detailed description in section 3.4.
3. Climatic changes concerning only land use changes or background climatic forcing are compared and analyzed by using differences under RCP45_2050_LND_S5_RCP45 and control experiments of CTL_RCP45_2050_LND_2000 and differences between other two CTL_RCP45_2050_LND_2000, CTL_RCP85_2050_LND_2000, and CTL_2000_LND_2000 scenarios, which are configured with the concentration variations of atmospheric GHGs and other radiative forcing constituents of two future RCP4.5 and RCP8.5 pathways by 2050 in contrast to the 20th century respectively; detailed comparisons in section 3.4.

The validation is carried out through comparison among WRF simulation with the land use map in 2000 and the two kinds of interpolated observational data as well as their pattern correlation assessment of average climatic variables in 2000 over whole China. As the observations used in the CRU TS data sets are fewer than the in situ data, the interpolated data from the in situ observations are of higher resolution and can highlight hot spots of local climatic change. The validation process uses initial and boundary conditions from the NCEP Final (FNL) analysis data achieved from the Global Forecast System with a 6-hr time interval at 1-degree resolution, which represents the current state of weather conditions well. The data are obtained from the Research Data Archive at the National Center for Atmospheric Research at http://rda.ucar.edu/ data sets /ds083.2/.

2.5. Land Use Datasets and Scenario Descriptions

A total of four land use data sets are used in the experiments. First, a newly aggregated land use map for 2000 is adopted. Since the original land use data of WRF have misclassifications such as overestimations of the urban areas in the Pearl River Delta (PRD; Chang et al., 2014; Li et al., 2014), underestimation of the broad-leaf and needleleaf forests, and misclassification of croplands in southern China (Liu et al., 2003; Situ et al., 2009), we replace the default surface land use with the newly generated 2000 land use map, which aggregates the Moderate Resolution Imaging Spectroradiometer (MODIS) International Geosphere-Biosphere Programme (IGBP) classification product and China Land-Use Monitoring (CLUM) data (Liu et al., 2010, 2014). The CLUM data are from the Chinese Academy of Science, which has more than 20 classes and is a complementary product to the MODIS product. Second, three 2050 land use maps illuminate disparate future land use developments under the comprehensive socioeconomic and emission pathways, which are simulated with six land use types (crop, urban, forest, shrub, grass, and other) by the ILUCM. To be consistent with the classes of the land surface model in WRF, land use from other sources should be harmonized and reclassified into the MODIS IGBP classification system, as shown in Table S1 in the supporting information.

We adopted the inverse distance weighting method, as suggested by (Lawrence & Chase, 2010), combined with present land cover data to realize the subdivision of classes, namely, the land use classes from the ILUCM simulation and the MODIS IGBP classes. In this research, we did not concern the effects of water management practices (e.g., irrigation) and inner land use emissions on land surface characters. Therefore, rather than focusing only on changes in the radiative properties of the land surface, our

experiments will also examine the energy and water exchanges between the surface and the atmosphere, which closely related to biogeophysical properties such as albedo, LAI, and surface roughness (Z_0).

Three future land use scenarios are combined by two representative socioeconomic pathways (SSP2 and SSP5) and two core emission pathways (RCP4.5 and RCP8.5). From previous research, land use data sets under those scenarios show significant characters of policy-induced impacts and differ largely in their spatial distributions (Dong et al., 2018). SSP2 represents a middle of the developing road and continuation of current trends in global socioeconomic development (O'Neill et al., 2014; van Vuuren et al., 2014). SSP5 denotes a scenario where countries put full focus on economic development, regardless of the environmental consequences (Dellink et al., 2017). SSP2 and SSP5 are comparable to evaluate distinctive land use-induced climate change due to the rapid economic growth and accompanying rising fossil fuel consumption in developing countries including China. To highlight the impacts due to climate mitigation policies, SSP5 is chosen as the same socioeconomic path to combine with those emission scenarios of RCP4.5 and RCP8.5 for comparisons. RCP 4.5 and 8.5 with significant difference in global radiative forcing levels result in different CO_2 concentration pathways to the end of the century. RCP8.5 with no explicit climate policy in emission mitigation pathway resulting in very high GHG emissions to more than 900 ppm is compared to RCP4.5, which adopt moderate carbon pricing policy as well as other technological changes stabilizing GHG emissions to about 550 ppm by 2100 (Brovkin et al., 2013). Socioeconomic factors such as the population, GDP, and urbanization ratio in SSP2 and SSP5 are shown in Figure 3a. The rapid increase of the national GDP and urbanization level under SSP5 makes urban and built-up areas of RCP45_2050_LND_S5_RCP45 and RCP85_2050_LND_S5_RCP85 increase faster compared to those of S2_2050 at the expense of cropland areas (Figure 3c). With the same socioeconomic levels as SSP5, RCP45_2050_LND_S5_RCP45 orienting to a moderate emission target of 4.5 W/m^2 in 2100 (Figure 3b) is found to have a gain in forest areas but a larger loss of grassland areas than those of RCP85_2050_LND_S5_RCP85 scenario, which gets reductions in both forest and grass areas and reaches to an extreme high radiative forcing of 8.5 W/m^2 in 2100 compared to the historical 2000 land use and climate conditions.

Spatial changes associated with the differences between each of the three future scenarios and the historical 2000 land use are presented in Figure 4, wherein some of the most noticeable expansion and shrinkage parts of land use types are indicated. These illustrate the possibilities of land use conditions after decadal interactions among land use and human activities and are far from idealized assumptions with land use changes at fixed locations. Dominant differences between land use of RCP45_2050_LND_S2_RCP45 and RCP45_2050_LND_S5_RCP45 are changes in urban areas and croplands as a result of socioeconomic drivers, whereas RCP45_2050_LND_S5_RCP45 and RCP85_2050_LND_S5_RCP85 exhibit the most distinguishable difference in the degree of forest expansion and grass degradation since RCP45_2050_LND_S5_RCP45 adopts a more powerful emission policy to obtain its mitigation target. Thus, the comparisons among land use changes under socioeconomic and emission scenarios enable a systematic investigation of human intervention on multiple land use types and their climatic impacts, as discussed in the following sections.

3. Results and Discussion

3.1. Model Evaluation

Previous research has shown that WRF performs well in regional climate simulations (Argüeso et al., 2014; Chen & Frauenfeld, 2016; Feng et al., 2012). Here we use both the CRU TS data and in situ observations to compare to the simulation results. Two meteorological parameters, the annual average air temperature at 2 m above the ground (T2) and the accumulated precipitation in summer (June to August) and winter (December to February) season of 2000, are examined (Figure 5). Also, pattern correlations are calculated with those three kinds of data for the area average temperature and precipitation in 2000 for the whole China to examine their similarity and differences.

Summer temperature from the simulation has pattern correlation coefficients of 0.96 and 0.84 with those from the CRU TS and the interpolated station data respectively, while the correlations for winter temperature are 0.96 and 0.91. As a whole, precipitation simulations indicate more bias than temperature, and the correlation coefficients are 0.77 and 0.74 in summer and 0.56 and 0.58 in winter. All correlation coefficients are statistically significant at the 99.9% confidence level. Larger biases in precipitation such as winter
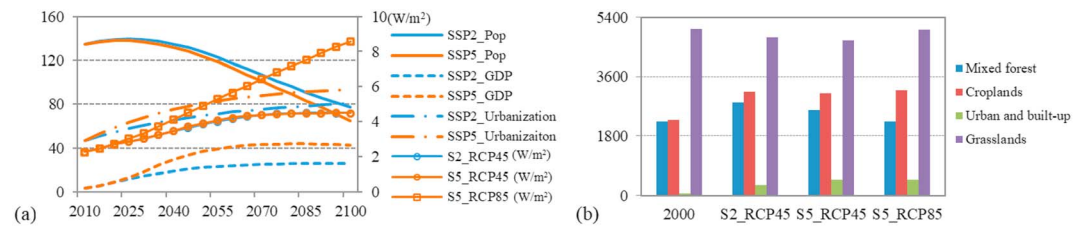
Figure 3. (a) The population (unit: ten million), gross domestic product (unit: trillion US$2005/year), and urbanization fraction (unit: %) trends in China under SSP2 and SSP5 scenarios and the global radiative forcing (W/m^2) under the three future scenarios (RCP45_2050_LND_S2_RCP45, RCP45_2050_LND_S5_RCP45, and RCP85_2050_LND_ S5_RCP85) from 2010 to 2100. (b) The different amounts of four land use types (the mixed forest, croplands, urban and built-up, and grasslands) among four land use data sets of the experiments, unit: thousand km^2.

underestimations in southeast and overestimations in southwest China may be attributed to the low level of precipitation amounts during dry season (Wang & Chen, 2014) and the convective and microphysical parameterization schemes (Chen & Frauenfeld, 2014a). Those validation results are comparable to those of Chen and Frauenfeld (2016). Overall, the agreement of WRF simulation with the two kinds of observational data sets demonstrates that the WRF model and its parameterizations capture the overall meteorological patterns well and are applicable to regional climate simulations. It is noticeable that relative large uncertainties exist for changes over the Tibetan Plateau because of few observations in that region, which could also account for the degrade performance of pattern correlation.
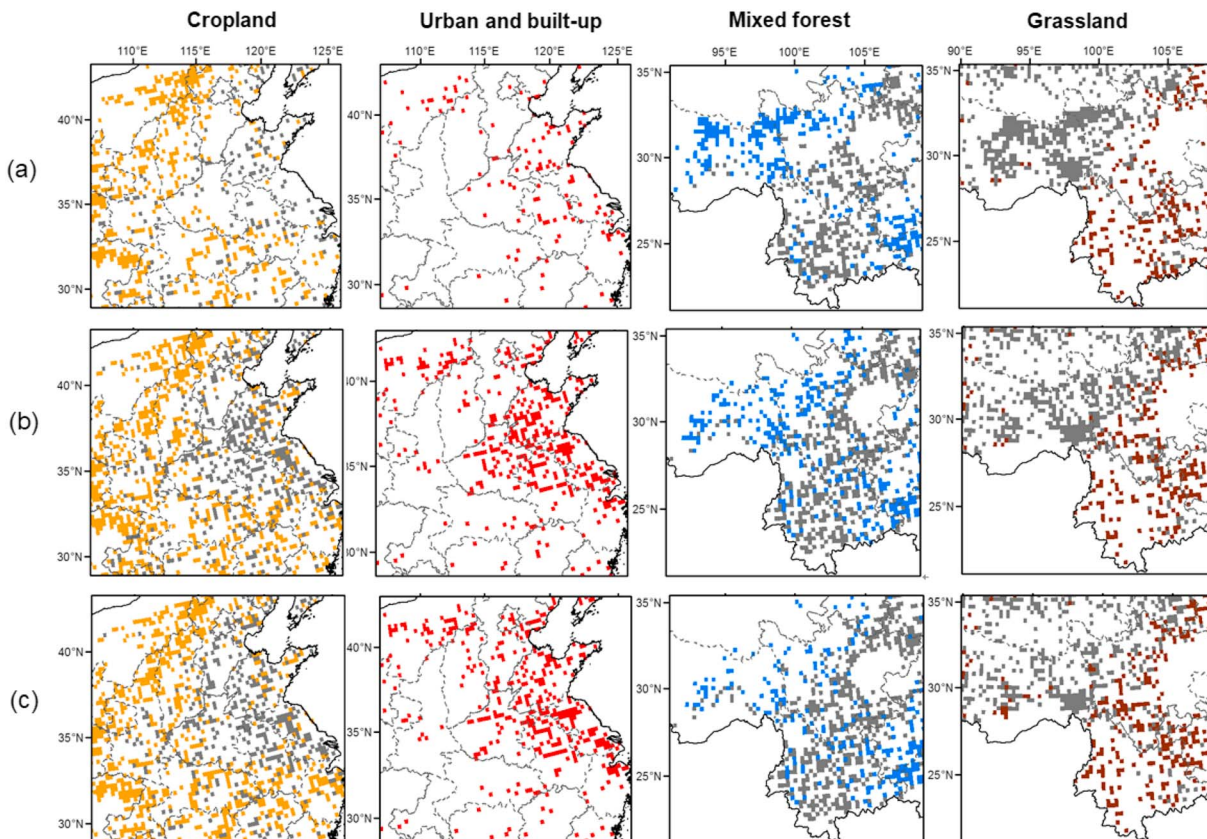
Figure 4. Examples of differences of cropland, urban and built-up, mixed forest and grassland distributions between land use data sets of (a) RCP45_2050_LND_S2_RCP45 and CTL_RCP45_2050_LND_2000, (b) RCP45_2050_LND_S5_RCP45 and CTL_RCP45_2050_LND_2000, and (c) RCP85_2050_LND_S5_RCP85 and CTL_RCP85_2050_LND_2000 experiments with pixels in grey representing decreases and other colors representing increases under the future scenarios. Specific locations of these examples in China are shown in Figure S1.
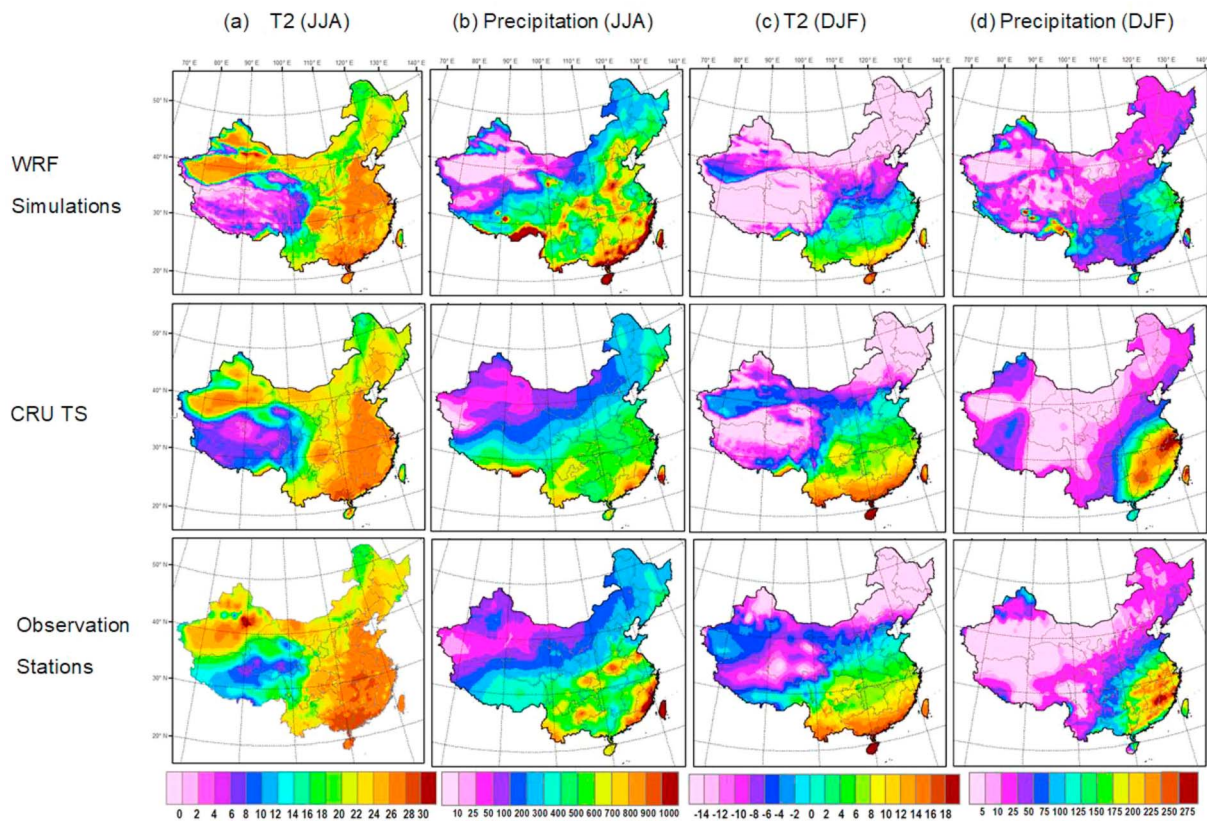
Figure 5. Comparison of the average (a) summer 2-m air temperature, (c) winter 2-m air temperature (unit: °C), (b) summer accumulated precipitation, and (d) winter accumulated precipitation (unit: mm) among Weather Research and Forecasting (WRF) simulations with the new 2000 land-use data (upper), CRU TS (middle), and Chinese observation stations (bottom) in 2000.

3.2. Future Land Use Impacts on Regional Climate
3.2.1. Socioeconomic Scenarios
3.2.1.1. (a) Land Use Changes and Effects on Meteorology

The most remarkable characteristic of the socioeconomic scenarios is the change in urban areas influenced by the population and GDP levels, which are proportional to the expansion speed of urbanization. Driven by SSP5 and SSP2, land use of RCP45_2050_LND_S5_RCP45 and RCP45_2050_LND_S2_RCP45 in China are both going to higher urbanization degree but less crop distribution around urbanized areas compared to 2000 land use of CTL_RCP45_2050_LND_2000 (Figure 6). Urbanization proportion is the larger in RCP45_2050_LND_S5_RCP45 than that in RCP45_2050_LND_S2_RCP45 as SSP5 scenario is under a higher developing speed. Desertification over north-western China occurs both in those two future socioeconomic scenarios compared to the condition of 2000. The most rapid increases of urbanization are concentrated in the Yangtze River Delta (YRD) and following the PRD and Beijing-Tianjin-Hebei (BTH) regions. Croplands expand along the boundary of the mixing zones for grasslands and the croplands from northeast to southwest Heihe-Tengchong line at the expense of grasslands under both RCP45_2050_LND_S2_RCP45 and RCP45_2050_LND_S5_RCP45 scenarios. Also, compared to the 2000 land use of CTL_RCP45_2050_LND_2000, the overall conversions of future land use in 2050s demonstrate more mixing and fragmented trends. In general, the two future socioeconomic scenarios generate consistent land use patterns but different conversion areas among various land use types due to differences in their level of social and economic development.

Accordingly, differences of 2-m air temperature and precipitation between each of the two socioeconomic scenarios and CTL_RCP45_2050_LND_2000 are uniquely affected by the land use changes, which exhibit similar spatial patterns (Figure 7). In general, the two land use changes under various socioeconomic development levels of RCP45_2050_LND_S2_RCP45 and RCP45_2050_LND_S5_RCP45 both induce overall
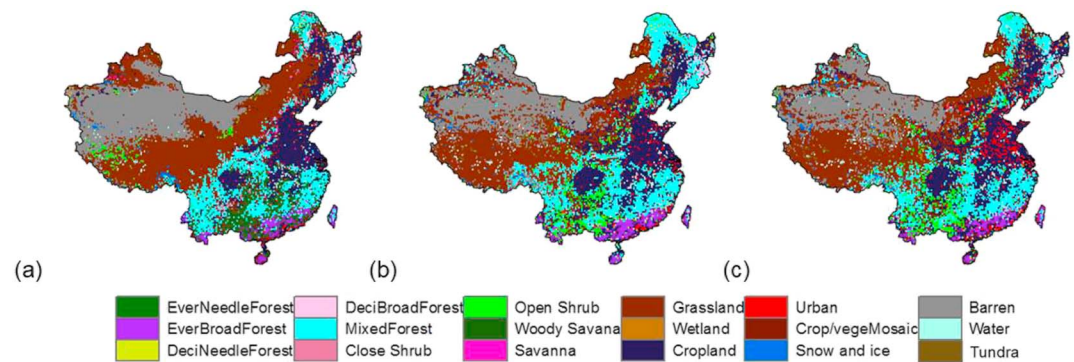
Figure 6. The land-use distributions of (a) CTL_RCP45_2050_LND_2000, (b) RCP45_2050_LND_S2_RCP45, and (c) RCP45_2050_LND_S5_RCP45.

climate warming in China compared to 2000 land use in CTL_RCP45_2050_LND_2000. RCP45_2050_LND_S5_RCP45 produces a larger maximum daily temperature (T_{max}) increase of 0.14°C but a smaller minimum daily temperature (T_{min}) rising of 0.13°C than temperature changes under RCP45_2050_LND_S2_RCP45 by 2050 (Figure S5). This quantitative results are comparable to that of Lin et al. (2016), which also found urban-induced warming in YRD, PRD, and BTH regions. However, land use change of RCP45_2050_LND_S2_RCP45 enhances average rainfall intensity of 0.11 mm/day, which is slightly more than RCP45_2050_LND_S5_RCP45 by 0.05 mm/day, compared to 2000 land use conditions of CTL_RCP45_2050_LND_2000. Therefore, the anthropogenic impacts of land use changes under the socioeconomic pathways driven by the population and the GDP levels of SSP5 and SSP2 would lead to a whole hotter and wetter climate in China by 2050.

Urbanization plays a decisive role in the heating processes with much different levels. Due to the large fraction of urbanization in the YRD, PRD, and BTH regions under RCP45_2050_LND_S5_RCP45, temperature increases significantly in summer with large areas passing t tests, whereas in winter only YRD and PRD have some areas with obvious warming effects. These findings partly agree with published results (Chen & Frauenfeld, 2016; Feng et al., 2012). A smaller increase in T_{min} and a larger increase in T_{max} under RCP45_2050_LND_S5_RCP45 leads to an overall larger DTR than those of RCP45_2050_LND_S2_RCP45,
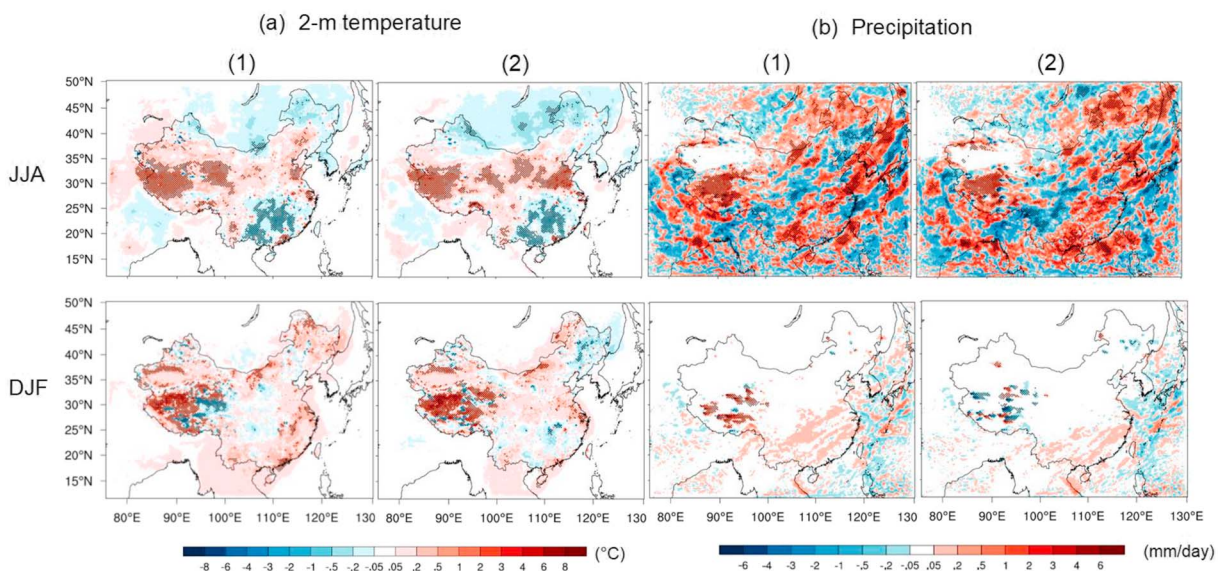
Figure 7. The differences in the average (a) 2-m temperature and (b) precipitation between (1) RCP45_2050_LND_S2_RCP45 and CTL_RCP45_2050_LND_2000 and (2) RCP45_2050_LND_S5_RCP45 and CTL_RCP45_2050_LND_2000 during summer (June-July-August [JJA]) and winter (December-January-February [DJF]). Regions with dots mean variations that have passed the significant t tests ($p<0.05$).

which undergoes lower level of urbanization, indicating that the nighttime heat release outweighs daytime heating arises from increased night surface heating and decreased evaporation by seasonal changes of vegetation and drier soil. Moreover, land use changes over northern China near the Inner Mongolia Province also promote summer warming, which is linked to forest and cropland extension over temperate and arid areas. In contrast, a cooler and wetter summer are found in the south and northeast China under both the RCP45_2050_LND_S2_RCP45 and RCP45_2050_LND_S5_RCP45 scenarios, mitigating the predominantly heating trends of urban areas. This is due to the extension of forests and shrublands converted from savannas and croplands.

3.2.1.2. (b) Geophysical Changes and Surface Heat Flux

The energy partitioning processes and change patterns caused by land use changes are almost the same except for over urbanization regions. Albedo shows opposite signals to LAI, which experiences a large increase in northeast and southern China as a result of the extension of forests and croplands in replacement from savannas and grasslands (Figure 8a). Latent heat flux (LHF) changes are consistent with LAI variation in southern China (Figure 8d) due to obvious natural vegetation conversions of savannas to forest and shrubs and increased evaporation under the warm and humid climate in tropical and subtropical zones. Urbanization areas show consistent change directions with albedo variations (Figure. 8b). Also, the albedo-driven sensible heat flux (SHF) changes show significant increases in YRD, PRD, and BTH regions, resulting in significant decreases in LHF and evaporation especially in RCP45_2050_LND_S5_RCP45 (Figure S2). Therefore, more obvious increased surface absorbed radiation of shortwave downward radiation (SWDOWN) greatly warms the surface air and increases summer temperature. As quantity changes of longwave downward radiation at surface (GLW) is small, total land surface radiation changes would be mainly affected by changes of SWDOWN and are in opposite symbols with humidity changes, showing a stronger decrease over southwestern China in RCP45_2050_LND_S5_RCP45 because of more water vapor rising into the air (Figure 8b and S2b).

3.2.2. Emission Scenarios

3.2.2.1. (a) Land Use Changes and Effects on Meteorology

Land use distributions of the two emissions scenarios with different radiative forcing targets (RCP4.5 and RCP8.5) are used to estimate possible climatic influences of climate mitigation policies. From the definition of the scenario (van Vuuren et al., 2011) and the adopted climate policy (universal carbon tax; see Wise et al., 2009), emission scenarios differ distinctively from the socioeconomic scenarios with the majority conversions of land use changes occurring between forests and other types as the rising carbon tax is beneficial to the forests and can improve the land capability for carbon storage. Urbanization under a rapid population and GDP development road of SSP5 determines that urban areas expand at fast speeds and demonstrate parallel spreading patterns at expense of croplands under both RCP45_2050_LND_S5_RCP45 and RCP85_2050_LND_S5_RCP85 (Figure 9). Compared to the historical 2000 land use data set, land use under the emission scenario of RCP45_2050_LND_S5_RCP45 applied climate mitigation policies and shows higher density of forestlands which arises in south, southwest, and northeast China. Cropland and shrub encroachment of grasslands occurs surrounding the mixing zone of grasslands and croplands along the northern Heihe-Tengchong line.

Due to differences in mitigation measures taken by these two emission scenarios, temperature, and precipitation under land use changes of RCP45_2050_LND_S5_RCP45 get warmer and wetter, while land use changes of RCP85_2050_LND_S5_RCP85 without any specific climate policy unexpectedly leads to slight increases and even decrease in summer temperature change (Figure 10a). Though RCP85_2050_LND_S5_RCP85 indicates an overall small gains in T_{avg} of 0.01°C compared to land use-induced impact from 2000, it exhibits extensive cooling effects over large parts of China but small warming over urbanization regions. Land-use of RCP45_2050_LND_S5_RCP45 with a similar urbanization level shows significant opposite symbols with RCP85_2050_LND_S5_RCP85 in southwest to north-central China. In this way, an overall increase of 0.09°C in summer temperature under RCP45_2050_LND_S5_RCP45 illustrates that warming effects over YRD, southern Inner Mongolia, and Gansu regions outweigh cooling effects over northeast and southern China. To the contrary, dominant cooling plays a decisive role in decreasing the average summer temperature to 0.09°C in RCP85_2050_LND_S5_RCP85. However, winter temperature changes over the two emission scenarios display consistent changes due to lower atmospheric temperature and weaker vegetation activities during winter.
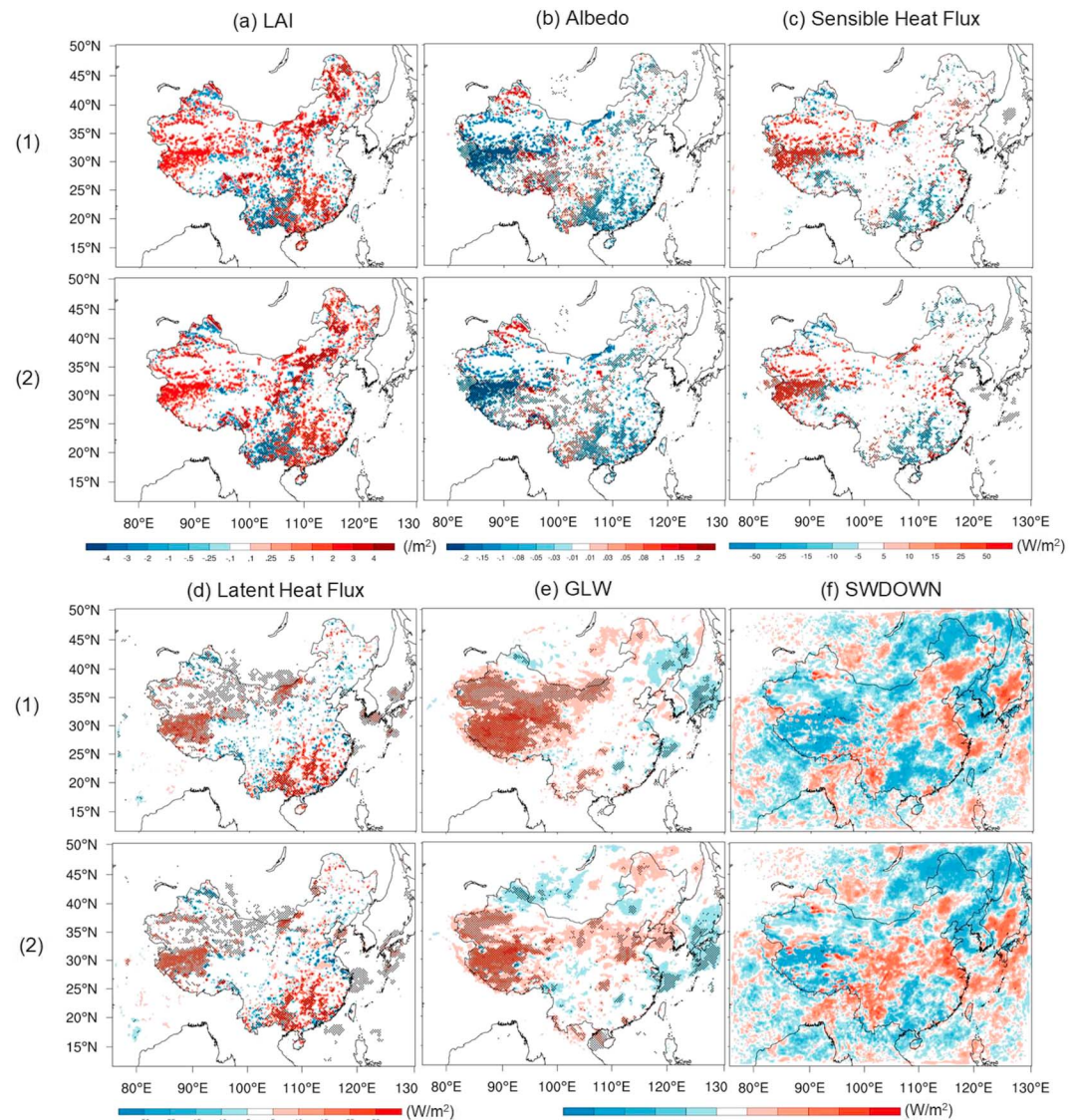
Figure 8. The differences in the average (a) leaf area index (LAI), (b) albedo, (c) sensible heat flux, (d) latent heat flux, (e) longwave downward radiation at surface (GLW), and (f) shortwave downward radiation at ground surface (SWDOWN) between (1) RCP45_2050_LND_S2_RCP45 and CTL_RCP45_2050_LND_2000 and (2) RCP45_2050_LND_S5_RCP45 and CTL_RCP45_2050_LND_2000 during summer. Regions with dots mean variations that have passed the significant *t* tests (*p*<0.05).

The summer precipitation under RCP45_2050_LND_S5_RCP45 has a stronger intensity of 0.13 mm/day rising than that under RCP85_2050_LND_S5_RCP85 as amount of forest increases in land use of RCP45_2050_LND_S5_RCP45 but decreases in RCP85_2050_LND_S5_RCP85 from 2000 land use (Figure 10b), indicating the positive role of reforestation in reducing the moisture loss into the atmosphere in the hot environment especially over northeast China. The effects on winter precipitation under two emission scenarios are almost the same in change patterns and make negligible contribution in the total precipitation change amounts.

3.2.2.2.   (b) Geophysical Changes and Surface Heat Flux
With a significant difference in climatic forcing and B/I conditions between RCP45_2050_LND_S5_RCP45 and RCP85_2050_LND_S5_RCP85, anthropogenic influences of the climatic policy-induced land use changes on regional climate is not only relevant to land properties such as LAI and albedo but also closed related to the background climate (Figure 11). Similar to the previous socioeconomic groups, LAI and albedo still show inverse trends but uniform spatial distributions due to the higher water content associated with
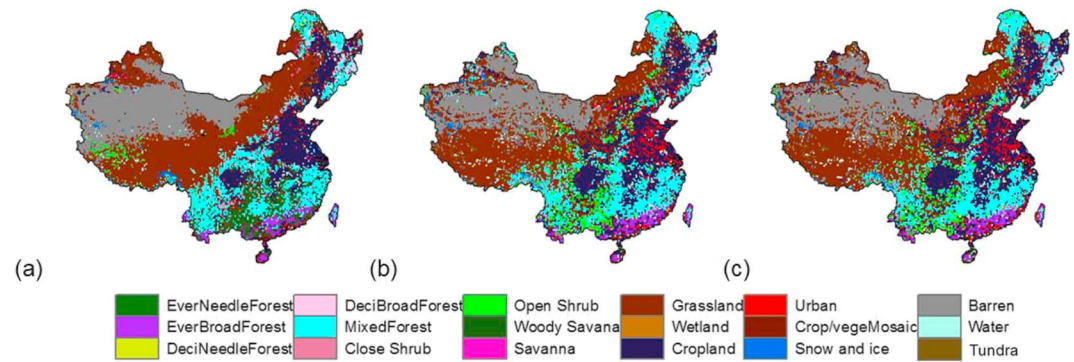
Figure 9. The land use distributions of (a) CTL_RCP45_2050_LND_2000/CTL_RCP85_2050_LND_2000, (b) RCP45_2050_LND_S5_RCP45, and (c) RCP85_2050_LND _S5_RCP85.

lower albedo in summer (Figure 11a and 11b). However, summer temperature changes induced by land use changes of RCP85_2050_LND_S5_RCP85 present slight larger increase in LHF over temperate zones from 27 to 40N with similar land use conversions of grasslands to croplands and forests. This would mainly contribute to the differences of background temperature under RCP8.5 and RCP4.5 as RCP8.5 with high GHG emission warms the whole atmospheric temperature and thus largely promote evaporations rates and LHF to cool the temperate zones (Figure 11d and S3). Zeng et al. (2017) also found that LAI-induced cooling from local vegetation could be masked under strong background climate circulations in East Asia. Under RCP8.5 conditions, Smith et al. (2017) indicated that increased evaporation and LHF would result in a small global cooling of 0.05°C. Additionally, stronger summer cooling occurs under RCP85_2050_LND_S5_RCP85 over southern China with corresponding large decrease in albedo and SFH resulted from land use conversions from grasslands to forests and shrubs (Figure 11b and 11c). GLW differences have similar characteristics with those of air temperature changes, while SWDOWN are closely correlated to water vapor and evaporation differences (Figure 11e and 11f).

Although evaporation is higher under RCP85_2050_LND_S5_RCP85, extreme background climate decreases summer precipitation in North China plain and northeast China and further strengthens precipitation over southern tropical and subtropical regions, causing a particular lower precipitation rising
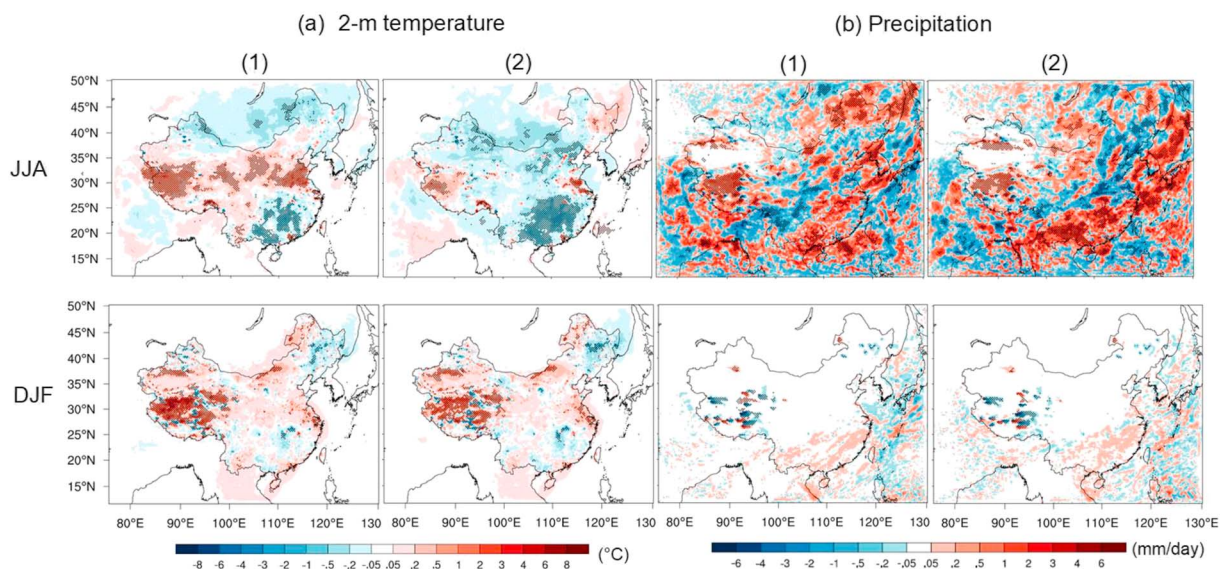
Figure 10. The differences in the average (a) 2-m temperature and (b) precipitation between (1) RCP45_2050_LND_S5_RCP45 and CTL_RCP45_2050_LND_2000 and (2) RCP85_2050_LND_S5_RCP85 and CTL_RCP85_2050_LND_2000 during summer (June-July-August [JJA]) and winter (December-January-February [DJF]). Regions with dots mean variations that have passed the significant *t* tests (*p*<0.05).
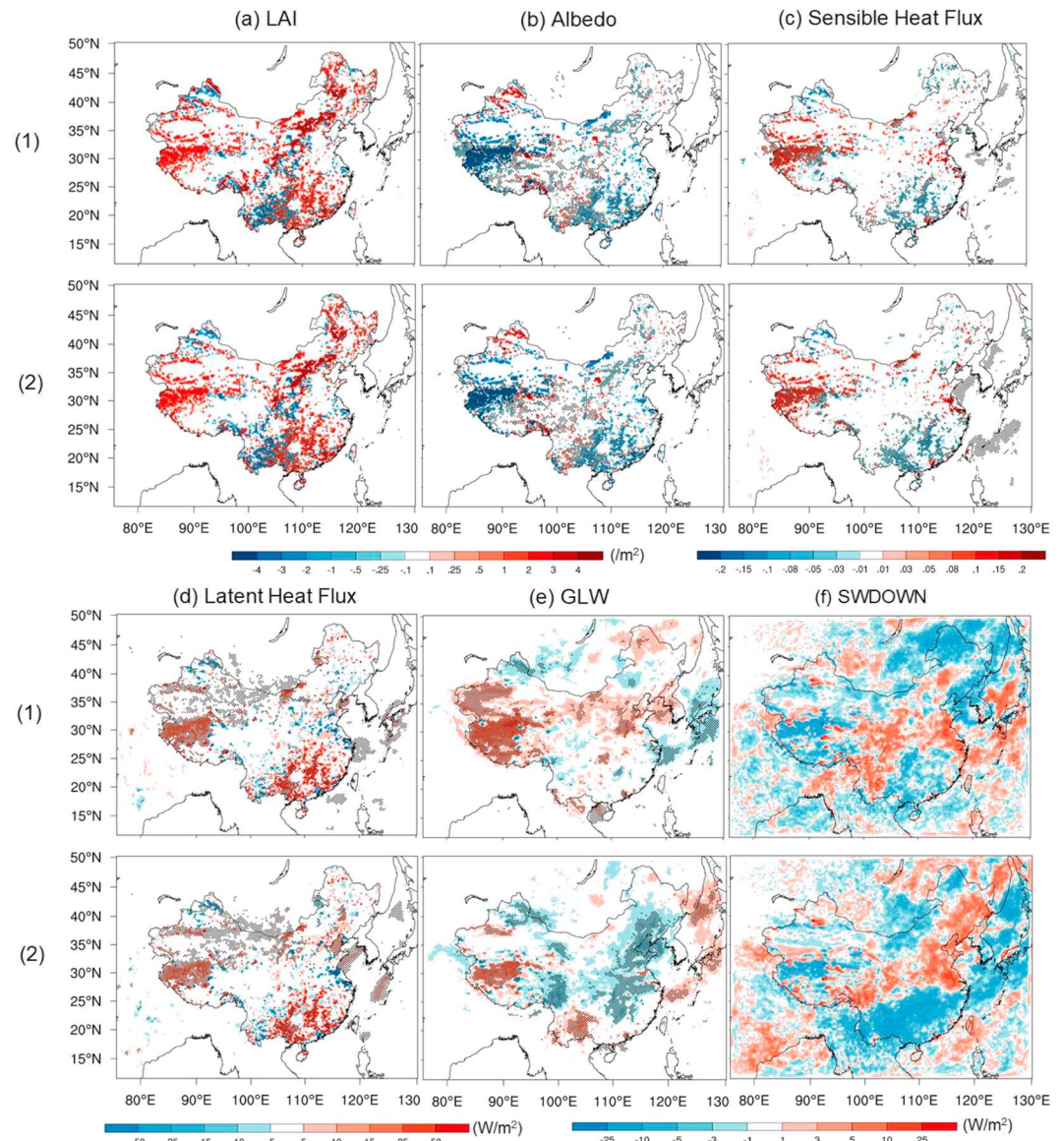
Figure 11. The differences in the average (a) leaf area index (LAI), (b) albedo, (c) sensible heat flux, (d) latent heat flux, (e) longwave downward radiation at surface (GLW), and (f) shortwave downward radiation at ground surface (SWDOWN) between (1) RCP45_2050_LND_S5_RCP45 and CTL_RCP45_2050_LND_2000 and (2) RCP85_2050_LND_S5_RCP85 and CTL_RCP85_2050_LND_2000 during summer. Regions with dots mean variations that have passed the significant *t* tests (*p*<0.05).

compared to changes brought by RCP45_2050_LND_S5_RCP45 (Figure S3). Urbanized regions subjected to outstanding decreases in LHF and increase in SHF changes demonstrate parallel reduction in summer precipitation and humidity (Figure S3b).

3.3. Comparison Among Impacts From Various Land Use Conversions and From Global Forcing

Net summer temperature changes induced by total land use area changes are extracted following the merged seven types (forest, shrub, grass, crop, urban, barren, and other) through the spatial statistics of temperature over those land use changed grids among those three groups of future experiments during summer (Figure 12a). Meanwhile, summer temperature change ratio per grid are calculated based on temperature changes occurring at each grid and each land use conversion from 2000 to 2050 to examine sensitivity and quantitative impacts of various land use changes to regional and local climate (Figure 12b). As the land
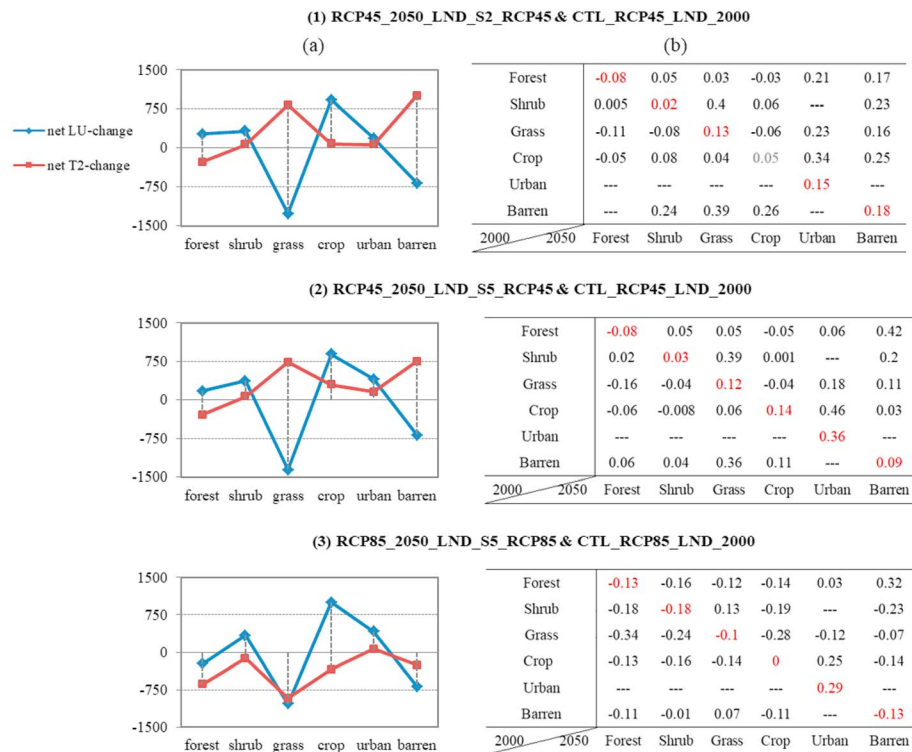
Figure 12. (a) Comparisons of net land-use change grids (unit: grid with 0.25-degree resolution) and their corresponding net summer temperature changes (unit: °C) over these areas of each land-use type (forest, shrub, grass, crop, urban, and barren) and (b) land use conversion induced summer temperature changes per grid among these six land use types from 2000 to 2050 under (1) RCP45_2050_LND_S2_RCP45 and CTL_RCP45_2050_LND_2000, (2) RCP45_2050_LND_S5_RCP45 and CTL_RCP45_2050_LND_2000, and (3) RCP85_2050_LND_S5_RCP85 and CTL_RCP85_2050_LND_2000. Temperatures in red are change from grids of each land-use type that keep the same in 2000 and 2050.

use type of other indicates snow and ice and is considered constant in the whole simulation period, we only involve the rest six land use types in comparisons of this part.

It is found that net land use changes are in similar direction among three groups except for forest changes under RCP85_2050_LND_S5_RCP85, which shows a decreased amount compared to 2000 land use. Meanwhile, net summer temperature changes of all land use type except for urban in RCP85_2050_LND_S5_RCP85 demonstrate cooling effects (Figure 12a). With few protective activities for forest growth, the high rate of economic development and extensive fossil fuel consumption in RCP85_2050_LND_S5_RCP85 result in a large reduction of forest converted to crop and grass. Extreme background forcing conditions increase total vegetation evaporation and LHF, thus cooling the surface. Corresponding temperature change ratios induced by land use change in RCP85_2050_LND_S5_RCP85 also differs much with the rest two in the opposite change directions of forest, shrub, grass, crop, and barren lands with a similar reason (Figure 12b). Changes in RCP45_2050_LND_S2_RCP45 and RCP45_2050_LND_S5_RCP45 have very consistent trends in all land use types but small differences in quantities of crop and urban lands, which come from their distinctive socioeconomic pathways adopted. Similarly, temperature change ratio caused by conversions from crop to urban, the most effective warming inducer followed by shrub to grass and barren to grass, is the higher in RCP45_2050_LND_S5_RCP45 and RCP85_2050_LND_S5_RCP85 than in RCP45_2050_LND_S2_RCP45 (Figure 12b). Greater degree of urbanization and socioeconomic development make significant contribution to land use conversions, which cools barren lands in RCP45_2050_LND_S5_RCP45 when it has the same amount of changed barren with that in RCP45_2050_LND_S2_RCP45. Among vegetation conversions, grass to forest brings the most obvious cooling while shrub to grass heats the land surface most. Therefore, it is hard to compare sensitivity of land use conversions in RCP85_2050_LND_S5_RCP85 group with other two groups. It is interesting to note that

Table 3
Comparison of Land Use Change and Climate Forcing (Background Atmospheric Impact) Induced Temperature (°C) and Precipitation (mm) Changes

Impact factor	ΔT_{max}	ΔT_{min}	ΔT_{avg}	ΔP_{avg}
Land-use change from 2050 SSP2&RCP45 to 2000 (RCP45_2050_LND_S2_RCP45-CTL_RCP45_2050_LND_2000)	0.12	0.15	0.14	0.11
Land-use change from 2050 SSP5&RCP45 to 2000 (RCP45_2050_LND_S5_RCP45-CTL_RCP45_2050_LND_2000)	0.14	0.13	0.14	0.06
Land-use change from 2050 SSP5&RCP85 to 2000 (RCP85_2050_LND _S5_RCP85-CTL_RCP85_2050_LND_2000)	0.02	-0.005	0.01	0.03
Climatic forcing from RCP45 to CMIP 20th century (CTL_RCP45_2050_LND_2000-CTL_2000_LND_2000)	1.20	1.44	1.27	0.21
Climatic forcing from RCP85 to CMIP 20th century (CTL_RCP85_2050_LND_2000-CTL_2000_LND_2000)	1.93	2.17	2.04	0.38

Abbreviations: CMIP, Coupled Model Intercomparison Project; RCP, Representative Concentration Pathway; SSP, Shared Socioeconomic Pathway.

temperature over those land use unchanged grids demonstrate evident warming in RCP45_2050_LND_S2_RCP45 and RCP45_2050_LND_S5_RCP45 but cooling in RCP85_2050_LND_S5_RCP85 (change ratios in red in Figure 12b), indicating that land use changes affect temperature over the local areas and even their surrounding areas such as the noticed rural warming around the urbanization expansion process.

As illustrated in Table 3, impacts from climatic forcing are much stronger than those from land use changes. Comparisons among two socioeconomic scenario groups of RCP45_2050_LND_S2_RCP45 and RCP45_2050_LND_S5_RCP45 observe increases in the ΔT_{avg} of a same 0.14°C and slight larger DTR occurs in the RCP45_2050_LND_S5_RCP45 with higher increase in ΔT_{max} and lower increase in ΔT_{min}. This is much smaller than the increase of 0.6-0.8°C reported in previous research (L. Chen & Frauenfeld, 2016), which only considered urbanization effects. The total ΔT_{avg} under RCP45_2050_LND_S5_RCP45, calculated from the total of land use change (0.14°C) and the climatic forcing (0.14°C), exhibits temperature change in 2050 would reach an average of 1.41°C higher than those in 2000 and increases at an annual rate of 0.028°C. This is comparable to the results of Chen and Frauenfeld (2014b) and Wang and Chen (2014), which are also related to future temperature changes in China driven by various RCP forcing data from the CMIP5 (Taylor et al., 2012) and the annual warming rates were assessed approximately 0.03 and 0.027°C, respectively, under RCP4.5 global forcing scenario. Climatic forcing of RCP8.5 causing completely greater warming in both ΔT_{max} and ΔT_{min} than that by RCP45 results in slight warming and even cooling effects from land use changes of RCP85_2050_LND_S5_RCP85. Precipitation enhanced by climatic forcing is twice or larger than that enhanced by land use changes, which would lead to a drier climate both due to extensive urbanization of RCP45_2050_LND_S5_RCP45 and climatic policies of RCP85_2050_LND_S5_RCP85. The heterogeneity and outstanding temperature change differences in local climate among specific regions such as eastern China, the Northeast China Plain, and South China (Figure S5) indicate that further detailed land use downscaling and delineation of climatic effect boundaries are urgently needed.

The significances in temperature differences under climatic forcing impacts almost spread the whole China and for most areas in precipitation differences, manifesting the strong regional effects caused by climatic forcing (Figure 13). Compared to land use change-induced seasonal temperature and precipitation in RCP45_2050_LND_S2_RCP45 (Figure 13, left), which displays a similar quantitative pattern with the other two future scenarios, global climatic forcing impacts under RCP4.5 and RCP8.5 condition (Figure 13, middle and right) both result in much warmer and wetter climate in China due to the rise of the global GHG concentration and other climatic variables for the initial and boundary conditions (details in https://rda.ucar.edu/datasets/ds316.1/). In addition, the variations of temperature and precipitation under climatic forcing impacts are more homogeneously distributed across space than land use induced effects, such as uniformed warming in temperature changes as well as spatial continuous amplified rainfall. The seasonal changes in temperature under influences of global climatic forcing would lead to remarkable extremes over the northeast and the Tibet Plateau, which are closely related to the increase in snow cover during winter.

The differences in climatic changes caused by the global climatic forcing other than land use can be further revealed by examining the process of energy and water exchanges (Figure S6 and S7). LHF that is dominated by comprehensive temperature and evaporation shows noticeable enhancement in the northeast to southern part of China due to strong warming from background climate. Albedo and
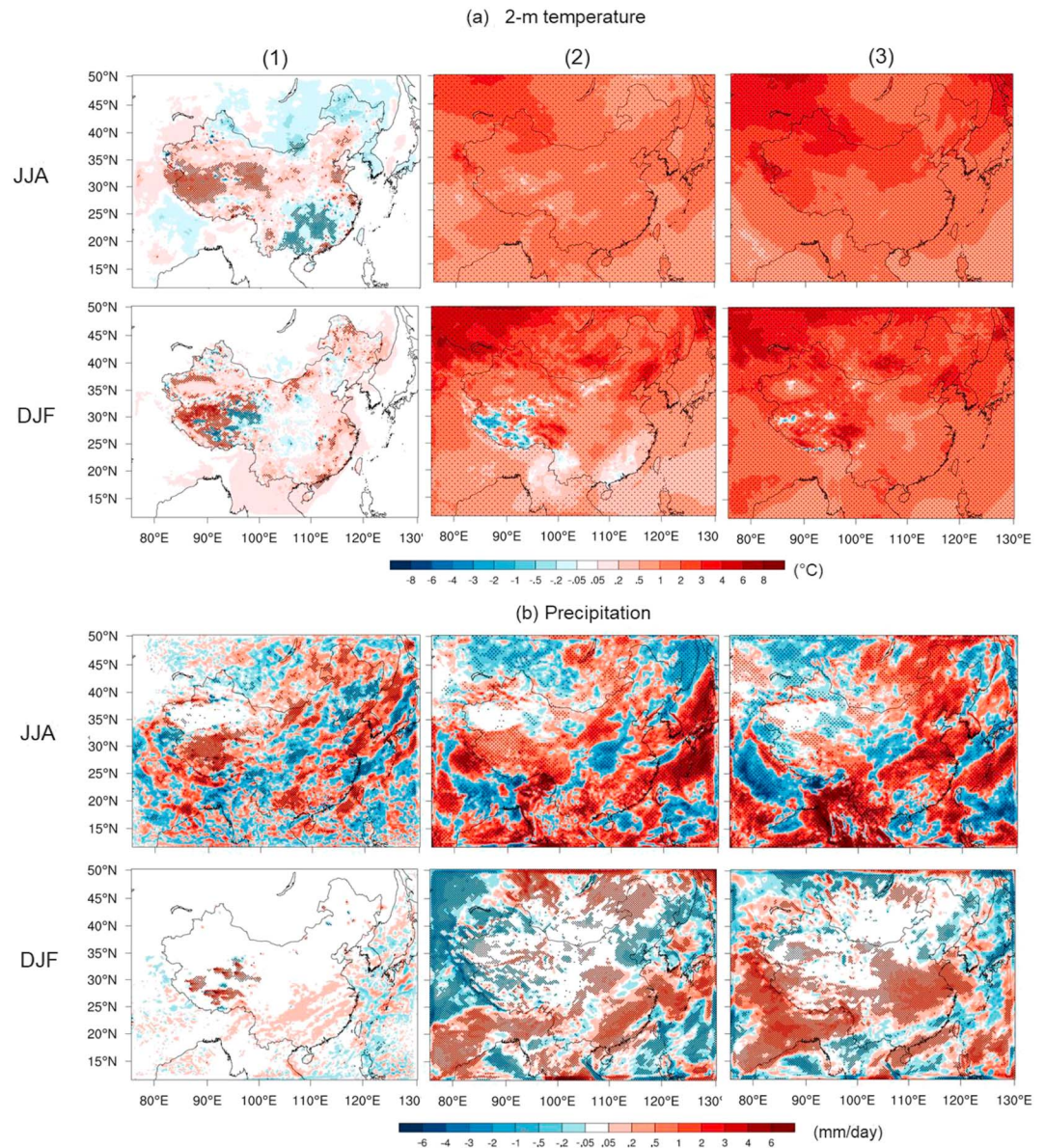
Figure 13. The differences in the average (a) 2-m temperature and (b) precipitation between the
(1) RCP45_2050_LND_S2_RCP45 and CTL_RCP45_2050_LND_2000, (2) CTL_RCP45_2050_LND_2000 and
CTL_2000_LND_2000, and (3) CTL_RCP85_2050_LND_2000 and CTL_2000_LND_2000 during summer (June-July-
August [JJA]) and winter (December-January-February [DJF[). Regions with dots mean variations that have passed the
significant t tests ($p<0.05$).

SHF relevant to surface properties exhibit smaller differences than LHF. As a whole, both evaporation
and humidity show great increases stimulated by the intensive precipitation, especially in summer, cor-
responding to the increase in the LHF over northeast China and the North China Plain.

4. Conclusion

In this study, we evaluate the effects of anthropogenic land use changes on climate in China under various
socioeconomic and emission scenarios by WRF simulation considering different land use data sets. Three
control scenarios of CTL_2000_LND_2000, CTL_RCP45_2050_LND_2000, and CTL_RCP85_2050_
LND_2000 with historical land use of 2000, and three future 2050 scenarios combining SSP2, SSP5, and
RCP4.5, RCP8.5 pathways are compared and analyzed in three ways. First, the variations in the near

surface air temperature dominated by urbanization under socioeconomic scenarios of RCP45_2050_LND_S5_RCP45 demonstrate significant increases in both T_{min} and T_{max}, and DTR originated from the warming effect of albedo and SHF changes. Second, the emission scenarios of RCP85_2050_LND_S5_RCP85 affected by the prominent urbanization and deforestation but suffering extreme high background warming indicate the lowest rising of T_{max} and T_{ave}, which are resulted from enhanced cooling of increased evaporation and LHF overperforming warming of decreased albedo and SHF under the very high RCP level. This finding is rarely be simulated and consistent with research of (Smith et al., 2017), which illustrated a small global cooling impact because of increased evaporation and LHF from surface. Temperature changes under the RCP4.5 scenario lead to a total increase of 1.41°C by 2050 at an annual rate of 0.028°C, consistent with the results of Chen and Frauenfeld (2014) and Wang and Chen (2014). Precipitation changes get toward drier climate with land use changes of more extensive urbanization and higher RCP effects in three future scenarios, displaying similar spatial patterns with a remarkable increase in south China and a decrease along the Heihe-Tengchong line adjacent to the croplands and grass conversion boundary during summer. Finally, with only climatic forcing, extreme high GHG emission and deeper disturbance to the precipitation pose greatly amplified effects on regional climate toward a warmer and wetter regime.

Besides the improvement in resolution, the combinations of SSP and RCP scenario in this research, considering effects of both emissions and diverse social development, for example, economic development and population growth, provide new ways to assess not only emissions but also societal impacts on global climate and environment change. Assessments only under RCPs could find regional changes under various global target pathways but without considering interactions between human society and environment, which can also be transferred to changes of surrounding environment. By contrast, with SSP scenarios different socioeconomic development for specific regions can be assembled with RCP targets to extend more comprehensive assumptions on anthropogenic impacts. In this research, we provide an integrated example on connections between land use changes (e.g., urbanization and forests) caused by divergent SSPs and RCPs and regional climate simulation to estimate potential regional climate variations under multiple anthropogenic forces.

However, the sensitivities of the simulated climate factors depend on the model mechanisms and parameters derived from the historical data such as albedo and LAI from the remote sensing images (Chen et al., 2010; Li et al., 2014). The assessment of regional climate responses requires promotion by utilizing finer and more accurate surface property data and observation data to assist the revelation of small-scale environmental changes. Additionally, improved understanding of the relationship between the land surface and atmosphere would be achieved by coupling the land and atmosphere modules in a dynamic way at a finer time scale to explore the detailed interactions underlying subsurface components and processes.

References

Adams, M., Duc, H., & Trieu, T. (2015). Impacts of land-use change on Sydney's future temperatures.

Argüeso, D., Evans, J. P., Fita, L., & Bormann, K. J. (2014). Temperature response to future urbanization and climate change. *Climate Dynamics*, *42*(7–8), 2183–2199. https://doi.org/10.1007/s00382-013-1789-6

Bonan, G. B. (2008). Forests and climate change: Forcings, feedbacks, and the climate benefits of forests. *Science.*. https://doi.org/10.1126/science.1155121

Bonan, G. B., Pollard, D., & Thompson, S. L. (1992). Effects of boreal forest vegetation on global climate. *Nature*, *359*(6397), 716–718. https://doi.org/10.1038/Doi, https://doi.org/10.1038/359716a0

Brovkin, V., Boysen, L., Arora, V. K., Boisier, J. P., Cadule, P., Chini, L., et al. (2013). Effect of anthropogenic land-use and land-cover changes on climate and land carbon storage in CMIP5 projections for the twenty-first century. *Journal of Climate*, *26*(18), 6859–6881. https://doi.org/10.1175/JCLI-D-12-00623.1

Brovkin, V., Claussen, M., Driesschaert, E., Fichefet, T., Kicklighter, D., Loutre, M. F., et al. (2006). Biogeophysical effects of historical land cover changes simulated by six Earth system models of intermediate complexity. *Climate Dynamics*, *26*(6), 587–600. https://doi.org/10.1007/s00382-005-0092-6

Cao, Q., Yu, D., Georgescu, M., & Wu, J. (2016). Impacts of urbanization on summer climate in China: An assessment with coupled land-atmospheric modeling. *Journal of Geophysical Research: Atmospheres*, *121*, 10,505–10,521. https://doi.org/10.1002/2016JD025210

Chang, M., Fan, S., & Wang, X. (2014). Impact of refined land-cover data on WRF performance over the Pearl River Delta region, China. *Huanjing Kexue Xuebao/Acta Scientiae Circumstantiae*, *34*(8), 1922–1933. https://doi.org/10.13671/j.hjkxxb.2014.0558

Chen, C., Park, T., Wang, X., Piao, S., Xu, B., Chaturvedi, R. K., et al. (2019). China and India lead in greening of the world through land-use management. *Nature Sustainability.*, *2*(2), 122–129. https://doi.org/10.1038/s41893-019-0220-7

Chen, F., & Dudhia, J. (2001). Coupling an advanced land surface – hydrology model with the Penn State–NCAR MM5 Modeling System. Part I: Model implementation and sensitivity. *Monthly Weather Review*, *129*(4), 569–585. https://doi.org/10.1175/1520-0493(2001)129<0569:caalsh>2.0.co;2

Chen, F., Kusaka, H., Bornstein, R., Ching, J., Grimmond, C. S. B., Grossman-Clarke, S., et al. (2011). The integrated WRF/urban modelling system: Development, evaluation, and applications to urban environmental problems. *International Journal of Climatology*, *31*(2), 273–288. https://doi.org/10.1002/joc.2158

Chen, L., & Frauenfeld, O. W. (2014a). A comprehensive evaluation of precipitation simulations over China based on CMIP5 multimodel ensemble projections. *Journal of Geophysical Research: Atmospheres*, *119*, 5767–5786. https://doi.org/10.1002/2013JD021190

Chen, L., & Frauenfeld, O. W. (2014b). Surface air temperature changes over the twentieth and twenty-first centuries in China simulated by 20 CMIP5 models. *Journal of Climate*, *27*(11), 3920–3937. https://doi.org/10.1175/JCLI-D-13-00465.1

Chen, L., & Frauenfeld, O. W. (2016). Impacts of urbanization on future climate in China. *Climate Dynamics*, *47*(1-2), 345–357. https://doi.org/10.1007/s00382-015-2840-6

Chen, Y., Yang, K., Zhou, D., Qin, J., & Guo, X. (2010). Improving the Noah Land Surface Model in arid regions with an appropriate parameterization of the thermal roughness length. *Journal of Hydrometeorology*, *11*(4), 995–1006. https://doi.org/10.1175/2010JHM1185.1

Clarke, L., Wise, M., Kim, S., Smith, S., & Lurz, J. (2007). Model documentation for the minicam climate change science program stabilization scenarios: Ccsp product 2.1 a. *Pacific Northwest National* (July). https://doi.org/PNNL-16735

Costa, M. H., & Foley, J. A. (2000). Combined effects of deforestation and doubled atmospheric CO2 concentrations on the climate of Amazonia. *Journal of Climate*, *13*(1), 18–34. https://doi.org/10.1175/1520-0442(2000)013<0018:CEODAD>2.0.CO;2

Davies-Barnard, T., Valdes, P. J., Singarayer, J. S., Wiltshire, A. J., & Jones, C. D. (2015). Quantifying the relative importance of land cover change from climate and land use in the representative concentration pathways. *Global Biogeochemical Cycles*, *29*, 842–853. https://doi.org/10.1002/2014GB004949

Davin, E. L., & de Noblet-Ducoudre, N. (2010). Climatic impact of global-scale Deforestation: Radiative versus nonradiative processes. *Journal of Climate*, *23*(1), 97–112. https://doi.org/10.1175/2009JCLI3102.1

Dellink, R., Chateau, J., Lanzi, E., & Magné, B. (2017). Long-term economic growth projections in the Shared Socioeconomic Pathways. *Global Environmental Change*, *42*, 200–214. https://doi.org/10.1016/j.gloenvcha.2015.06.004

Deng, X., Zhao, C., Lin, Y., Zhang, T., Qu, Y., Zhang, F., et al. (2014). Downscaling the impacts of large-scale LUCC on surface temperature along with IPCC RCPs: A global perspective. *Energies*, *7*(4), 1852–1875. https://doi.org/10.3390/en7041852

de Noblet-Ducoudré, N., Boisier, J. P., Pitman, A., Bonan, G. B., Brovkin, V., Cruz, F., et al. (2012). Determining robust impacts of land-use-induced land cover changes on surface climate over North America and Eurasia: Results from the first set of LUCID experiments. *Journal of Climate*, *25*(9), 3261–3281. https://doi.org/10.1175/JCLI-D-11-00338.1

Dong, N., You, L., Cai, W., Li, G., & Lin, H. (2018). Land use projections in China under global socioeconomic and emission scenarios: Utilizing a scenario-based land-use change assessment framework. *Global Environmental Change*, *50*, 164–177. https://doi.org/10.1016/j.gloenvcha.2018.04.001

Fall, S., Niyogi, D., Gluhovsky, A., Pielke, R. A., Kalnay, E., & Rochon, G. (2010). Impacts of land use land cover on temperature trends over the continental United States: Assessment using the North American Regional Reanalysis. *International Journal of Climatology*, *30*(13), 1980–1993. https://doi.org/10.1002/joc.1996

Feng, J. M., Wang, Y. L., Ma, Z. G., & Liu, Y. H. (2012). Simulating the regional impacts of urbanization and anthropogenic heat release on climate across China. *Journal of Climate*, *25*(20), 7187–7203. https://doi.org/10.1175/JCLI-D-11-00333.1

Findell, K. L., Berg, A., Gentine, P., Krasting, J. P., Lintner, B. R., Malyshev, S., et al. (2017). The impact of anthropogenic land use and land cover change on regional climate extremes. *Nature Communications*, *8*(1), 989. https://doi.org/10.1038/s41467-017-01038-w

Foley, J. A. (2005). Global consequences of land use. *Science*, *309*(5734), 570–574. https://doi.org/10.1126/science.1111772

Georgescu, M., Lobell, D. B., & Field, C. B. (2011). Direct climate effects of perennial bioenergy crops in the United States. *Proceedings of the National Academy of Sciences*, *108*(11), 4307–4312. https://doi.org/10.1073/pnas.1008779108

Govindasamy, B., Duffy, P. B., & Caldeira, K. (2001). Land use changes and Northern Hemisphere cooling. *Geophysical Research Letters*, *28*(2), 291–294. https://doi.org/10.1029/2000GL006121

Grossman-Clarke, S., Zehnder, J. A., Loridan, T., & Grimmond, C. S. B. (2010). Contribution of land use changes to near-surface air temperatures during recent summer extreme heat events in the Phoenix metropolitan area. *Journal of Applied Meteorology and Climatology*, *49*(8), 1649–1664. https://doi.org/10.1175/2010JAMC2362.1

Hale, R. C., Gallo, K. P., & Loveland, T. R. (2008). Influences of specific land use/land cover conversions on climatological normals of near-surface temperature. *Journal of Geophysical Research*, *113*, D14113. https://doi.org/10.1029/2007JD009548

Hale, R. C., Gallo, K. P., Owen, T. W., Loveland, T. R. (2006). Land use/land cover change effects on temperature trends at U.S. Climate Normals stations. *Geophysical Research Letters*, *33*. L11703. https://doi.org/10.1029/2006GL026358

Harris, I., Jones, P. D., Osborn, T. J., & Lister, D. H. (2014). Updated high-resolution grids of monthly climatic observations - the CRU TS3.10 Dataset. *International Journal of Climatology*, *34*(3), 623–642. https://doi.org/10.1002/joc.3711

Hong, S., Lakshmi, V., Small, E. E., Chen, F., Tewari, M., & Manning, K. W. (2009). Effects of vegetation and soil moisture on the simulated land surface processes from the coupled WRF/Noah model. *Journal of Geophysical Research*, *114*, D18118. https://doi.org/10.1029/2008JD011249

Hurtt, G. C., Chini, L. P., Frolking, S., Betts, R. A., Feddema, J., Fischer, G., et al. (2011). Harmonization of land-use scenarios for the period 1500-2100: 600 years of global gridded annual land-use transitions, wood harvest, and resulting secondary lands. *Climatic Change*, *109*(1-2), 117–161. https://doi.org/10.1007/s10584-011-0153-2

International Panel on Climate Change. (2013). IPCC Fifth Assessment Report (AR5). IPCC.

Jeong, S. J., Ho, C. H., Piao, S., Kim, J., Ciais, P., Lee, Y. B., et al. (2014). Effects of double cropping on summer climate of the North China Plain and neighbouring regions. *Nature Climate Change*, *4*(7), 615–619. https://doi.org/10.1038/nclimate2266

Kim, S. H., Edmonds, J., Lurz, J., Smith, S. J., & Wise, M. (2006). The O bj ECTS Framework for Integrated Assessment: Hybrid modeling of transportation. *The Energy Journal*, *Sl2005*(01).

Kusaka, H., & Kimura, F. (2004). Thermal effects of urban canyon structure on the nocturnal heat island: Numerical experiment using a mesoscale model coupled with an urban canopy model. *Journal of Applied Meteorology*, *43*(12), 1899–1910. https://doi.org/10.1175/JAM2169.1

Lai, L., Huang, X., Yang, H., Chuai, X., Zhang, M., Zhong, T., et al. (2016). Carbon emissions from land-use change and management in China between 1990 and 2010. *Science Advances*, *2*(11), 1–9. https://doi.org/10.1126/sciadv.1601063

Lawrence, P. J., & Chase, T. N. (2010). Investigating the climate impacts of global land cover change in the community climate system model. *International Journal of Climatology*, *30*(13), 2066–2087. https://doi.org/10.1002/joc.2061

Li, M., Song, Y., Huang, X., Li, J., Mao, Y., Zhu, T., et al. (2014). Improving mesoscale modeling using satellite-derived land surface parameters in the Pearl River Delta region, China. *Journal Of Geophysical Research: Atmospheres*, *119*, 6325–6346. https://doi.org/10.1002/2014JD021871

Li, X., Chen, G., Liu, X., Liang, X., Wang, S., Chen, Y., et al. (2017). A new global land-use and land-cover change product at a 1-km resolution for 2010 to 2100 based on human–environment interactions. *Annals of the American Association of Geographers*, *107*(5), 1040–1059. https://doi.org/10.1080/24694452.2017.1303357

Li, Y., Li, Z., Li, Z., Geng, X., & Deng, X. (2013). Numerical simulation of the effects of grassland degradation on the surface climate in overgrazing area of Northwest China. *Advances in Meteorology*, *2013*, 1–9. https://doi.org/10.1155/2013/270192

Lin, S., Feng, J., Wang, J., & Hu, Y. (2016). Modeling the contribution of long-term urbanization to temperature increase in three extensive urban agglomerations in China. *Journal of Geophysical Research: Atmospheres*, *121*, 1683–1697. https://doi.org/10.1002/2015JD024227

Liu, J., Kuang, W., Zhang, Z., Xu, X., Qin, Y., Ning, J., et al. (2014). Spatiotemporal characteristics, patterns and causes of land use changes in China since the late 1980s. *Journal of Geographical Sciences*, *24*(2), 195–210. https://doi.org/10.11821/dlxb201401001

Liu, J., Liu, M., Zhuang, D., Zhang, Z., & Deng, X. (2003). Study on spatial pattern of land-use change in China during 1995–2000. *Science in China Series D*, *46*(4), 373–384. https://doi.org/10.1360/03yd9033

Liu, J., Zhang, Z., Xu, X., Kuang, W., Zhou, W., Zhang, S., et al. (2010). Spatial patterns and driving forces of land use change in China during the early 21st century. *Journal of Geographical Sciences*, *20*(4), 483–494. https://doi.org/10.1007/s11442-010-0483-4

Liu, X., Liang, X., Li, X., Xu, X., Ou, J., Chen, Y., et al. (2017). A future land use simulation model (FLUS) for simulating multiple land use scenarios by coupling human and natural effects. *Landscape and Urban Planning*, *168*, 94–116. https://doi.org/10.1016/j.landurbplan.2017.09.019

Luo, M., & Lau, N. C. (2017). Heat waves in southern China: Synoptic behavior, long-term change, and urbanization effects. *Journal of Climate*, *30*(2), 703–720. https://doi.org/10.1175/JCLI-D-16-0269.1

Mahmood, R., Hubbard, K. G., Leeper, R. D., & Foster, S. A. (2008). Increase in near-surface atmospheric moisture content due to land use changes: Evidence from the observed dewpoint temperature data. *Monthly Weather Review*, *136*(4), 1554–1561. https://doi.org/10.1175/2007MWR2040.1

Mahmood, R., Pielke, R. A. Sr., Hubbard, K. G., Niyogi, D., Bonan, G., Lawrence, P., et al. (2010). Impacts of land use/land cover change on climate and future research priorities. *Bulletin of the American Meteorological Society*, *91*(1), 37–46. https://doi.org/10.1175/2009BAMS2769.1

Matthews, H. D., Weaver, A. J., Eby, M., & Meissner, K. J. (2003). Radiative forcing of climate by historical land cover change. *Geophysical Research Letters*, *30*(2), 1055. https://doi.org/10.1029/2002GL016098

Monaghan, A. J., Steinhoff, D. F., Bruyere, C. L., & Yates, D. (2014). *NCAR CESM Global Bias-Corrected CMIP5 Output to Support WRF/MPAS Research*. Research Data Archive at the National Center for Atmospheric Research, Computational and Information Systems Laboratory, Boulder, Colo. Accessed 25 03 2018. https://doi.org/10.5065/D6DJ5CN4

Moss, R. H., Edmonds, J. A., Hibbard, K. A., Manning, M. R., Rose, S. K., van Vuuren, D. P., et al. (2010). The next generation of scenarios for climate change research and assessment. *Nature*, *463*(7282), 747–756. https://doi.org/10.1038/nature08823

Oleson, K. W., Monaghan, A., Wilhelmi, O., Barlage, M., Brunsell, N., Feddema, J., et al. (2015). Interactions between urbanization, heat stress, and climate change. *Climatic Change*, *129*(3–4), 525–541. https://doi.org/10.1007/s10584-013-0936-8

O'Neill, B. C., Kriegler, E., Ebi, K. L., Kemp-Benedict, E., Riahi, K., Rothman, D. S., et al. (2017). The roads ahead: Narratives for shared socioeconomic pathways describing world futures in the 21st century. *Global Environmental Change*, *42*, 169–180. https://doi.org/10.1016/j.gloenvcha.2015.01.004

O'Neill, B. C., Kriegler, E., Riahi, K., Ebi, K. L., Hallegatte, S., Carter, T. R., et al. (2014). A new scenario framework for climate change research: The concept of shared socioeconomic pathways. *Climatic Change*, *122*(3), 387–400. https://doi.org/10.1007/s10584-013-0905-2

Pielke, R. A., & Niyogi, D. (2010). The role of landscape processes within the climate system. In *Lecture Notes in Earth Sciences*, (Vol. 115, pp. 67–85). Springer. https://doi.org/10.1007/978-3-540-75761-0_5

Pielke, R. A., Adegoke, J., Beltrán-Przekurat, A., Hiemstra, C. A., Lin, J., Nair, U. S., & Nobis, T. E. (2007). An overview of regional land-use and land-cover impacts on rainfall. *Tellus, Series B: Chemical and Physical Meteorology*, *59*, 587–601. https://doi.org/10.1111/j.1600-0889.2007.00251.x

Ren, G., Zhou, Y., Chu, Z., Zhou, J., Zhang, A., Guo, J., & Liu, X. (2008). Urbanization effects on observed surface air temperature trends in North China. *Journal of Climate*, *21*(6), 1333–1348. https://doi.org/10.1175/2007JCLI1348.1

Riahi, K., Rao, S., Krey, V., Cho, C., Chirkov, V., Fischer, G., et al. (2011). RCP 8.5-A scenario of comparatively high greenhouse gas emissions. *Climatic Change*, *109*(1-2), 33–57. https://doi.org/10.1007/s10584-011-0149-y

Rounsevell, M. D. A., Arneth, A., Alexander, P., Brown, D. G., de Noblet-Ducoudré, N., Ellis, E., et al. (2014). Towards decision-based global land use models for improved understanding of the Earth system. *Earth System Dynamics*, *5*(1), 117–137. https://doi.org/10.5194/esd-5-117-2014

Roy, S. S., Mahmood, R., Niyogi, D., Lei, M., Foster, S. A., Hubbard, K. G., et al. (2007). Impacts of the agricultural Green Revolution-induced land use changes on air temperatures in India. *Journal of Geophysical Research*, *112*, D21108. https://doi.org/10.1029/2007JD008834

Skamarock, W. C., Klemp, J. B., Gill, D. O., Barker, D.M., & Powers, J. G. (2005). *June 2005 A Description of the Advanced Research WRF Version 2. NCAR Tech. Note NCAR/TN-475+ STR* (p. 113).

Skamarock, W. C., Wang, W., Klemp, J. B., Dudhia, J, Gill, D. O., Barker, D. M, & Powers, J. G. (2008). *2005: A Description of the Advanced Research WRF Version 3. NCAR Tech Note* (pp. 488–494).

Situ, S. P., & WangXM, A. (2009). Typical summertime isoprene emission from vegetation in the Pearl River Delta region, China [J]. *Acta Science Circumstantiae*, *29*(4), 822–829. (In Chinese)

Smith, N. G., Lombardozzi, D., Tawfik, A., Bonan, G., & Dukes, J. S. (2017). Biophysical consequences of photosynthetic temperature acclimation for climate. *Journal of Advances in Modeling Earth Systems*, *9*, 536–547. https://doi.org/10.1002/2016MS000732

Taylor, K. E., Stouffer, R. J., & Meehl, G. A. (2012). An overview of CMIP5 and the experiment design. *Bulletin of the American Meteorological Society*, *93*(4), 485–498. https://doi.org/10.1175/BAMS-D-11-00094.1

Teuling, A. J., Seneviratne, S. I., Stöckli, R., Reichstein, M., Moors, E., Ciais, P., et al. (2010). Contrasting response of European forest and grassland energy exchange to heatwaves. *Nature Geoscience*, *3*(10), 722–727. https://doi.org/10.1038/ngeo950

Thomson, A. M., Calvin, K. V., Smith, S. J., Kyle, G. P., Volke, A., Patel, P., et al. (2011). RCP4.5: A pathway for stabilization of radiative forcing by 2100. *Climatic Change*, *109*(1-2), 77–94. https://doi.org/10.1007/s10584-011-0151-4

van Vuuren, D. P., Edmonds, J., Kainuma, M., Riahi, K., Thomson, A., Hibbard, K., et al. (2011). The representative concentration pathways: An overview. *Climatic Change*, *109*(1-2), 5–31. https://doi.org/10.1007/s10584-011-0148-z

van Vuuren, D. P., Kriegler, E., O'Neill, B. C., Ebi, K. L., Riahi, K., Carter, T. R., et al. (2014). A new scenario framework for Climate Change Research: Scenario matrix architecture. *Climatic Change*, *122*(3), 373–386. https://doi.org/10.1007/s10584-013-0906-1

Wang, J., Feng, J., Yan, Z., Hu, Y., & Jia, G. (2012). Nested high-resolution modeling of the impact of urbanization on regional climate in three vast urban agglomerations in China. *Journal of Geophysical Research*, *117*, D21103. https://doi.org/10.1029/2012JD018226

Wang, L., & Chen, W. (2014). A CMIP5 multimodel projection of future temperature, precipitation, and climatological drought in China. *International Journal of Climatology*, *34*(6), 2059–2078. https://doi.org/10.1002/joc.3822

Ward, D. S., Mahowald, N. M., & Kloster, S. (2014). Potential climate forcing of land use and land cover change. *Atmospheric Chemistry and Physics*, *14*(23), 12701–12724. https://doi.org/10.5194/acp-14-12701-2014

Wise, M., & Calvin, K. (2011). GCAM 3.0 agriculture and land use modeling: Technical description of modeling approach, (20971). Retrieved from https://wiki.umd.edu/gcam/images/8/87/GCAM3AGTechDescript12_5_11.pdf

Wise, M., Calvin, K., Thomson, A., Clarke, L., Bond-Lamberty, B., Sands, R., et al. (2009). Implications of limiting CO_2 concentrations for land use and energy. *Science*, *324*(5931), 1183–1186. https://doi.org/10.1126/science.1168475

Yang, L., Niyogi, D., Tewari, M., Aliaga, D., Chen, F., Tian, F., & Ni, G. (2016). Contrasting impacts of urban forms on the future thermal environment: Example of Beijing metropolitan area. *Environmental Research Letters*, *11*(3). https://doi.org/10.1088/1748-9326/11/3/034018

Zeng, Z., Piao, S., Li, L. Z. X., Zhou, L., Ciais, P., Wang, T., et al. (2017). Climate mitigation from vegetation biophysical feedbacks during the past three decades. *Nature Climate Change*, *7*(6), 432–436. https://doi.org/10.1038/nclimate3299

Zhou, L., Dickinson, R. E., Tian, Y., Fang, J., Li, Q., Kaufmann, R. K., et al. (2004). Evidence for a significant urbanization effect on climate in China. *Proceedings of the National Academy of Sciences*, *101*(26), 9540–9544. https://doi.org/10.1073/pnas.0400357101